

1 **Coupling of CpCr(CO)₃ and Heterocyclic Dithiadiazolyl Radicals. Synthetic, X-ray**
2 **diffraction, dynamic NMR, EPR, CV and DFT studies.**

3
4 Hiu Fung Lau,^(a) Pearly Chwee Ying Ang,^(a) Victor Wee Lin Ng,^(a) Seah Ling Kuan,^(a) Lai Yoong
5 Goh,^{(a)*†} Alexey S. Borisov,^(b) Paul Hazendonk,^(b) Tracey L. Roemmele,^(b) René T. Boéré,^{(b)*‡}
6 and Richard D. Webster^(c)

7
8 ^(a) *Department of Chemistry, National University of Singapore, Kent Ridge, Singapore 119260*

9 ^(b) *Department of Chemistry and Biochemistry, University of Lethbridge, Lethbridge, Alberta,*
10 *Canada T1K 3M4*

11 ^(c) *Division of Chemistry and Biological Chemistry, School of Physical & Mathematical*
12 *Sciences, Nanyang Technological University, Singapore 637371*

13
14 † Present address: Division of Chemistry and Biological Chemistry, School of Physical and
15 Mathematical Sciences, Nanyang Technological University, Singapore 637371. Email:
16 LaiYoongGoh@ntu.edu.sg. Fax +65 6316 6984

17 ‡ Email: boere@uleth.ca. Fax: +1-403-329-2057

20 **Abstract**

21 The reaction of 1,2,3,5-dithiadiazolyls, (4-R-C₆H₄CN₂S₂)₂ (R = Me, **2a**; Cl, **2b**; OMe, **2c**; and
22 CF₃, **2d**) and (3-NC-5-^tBu-C₆H₃CN₂S₂)₂ (**2e**) with (CpCr(CO)₃)₂ (Cp = η⁵-C₅H₅) (**1**) at ambient
23 temperature, yielded respectively the complexes CpCr(CO)₂(η²-S₂N₂CC₆H₄R) (R = 4-Me, **3a**; 4-
24 Cl, **3b**; 4-OMe, **3c**; and 4-CF₃, **3d**) and CpCr(CO)₂(η²-S₂N₂CC₆H₃-3-(CN)-5-(^tBu)) (**3e**) in 35 –
25 72 % yields. The complexes **3c** and **3d** were also synthesized via a salt metathesis method from
26 the reaction of NaCpCr(CO)₃ (**1B**) and the 1,2,3,5-dithiadiazolium chlorides, 4-R-C₆H₄CN₂S₂Cl
27 (R = OMe, **8c**; CF₃, **8d**) with much lower yields of 6 and 20 %, respectively. The complexes
28 were characterized spectroscopically, and also by single crystal X-ray diffraction analysis. Cyclic
29 voltammetry experiments were conducted on **3a-e**, EPR spectra were obtained of one-electron
30 reduced forms of **3a-e**, and variable temperature ¹H NMR studies were carried out on complex
31 **3d**. Hybrid DFT calculations were performed on the model system [CpCr(CO)₂S₂N₂CH] and
32 comparisons are made with the reported CpCr(CO)₂(π-allyl) complexes.

33

34 **Keywords:** *dithiadiazolyl, organometallic radical, C,N,S-heterocyclic radicals, cyclopentadienyl*
35 *chromium, π-complexes of C,N,S-heterocyclic rings, X-ray structural, CV, EPR and*
36 *computational studies.*

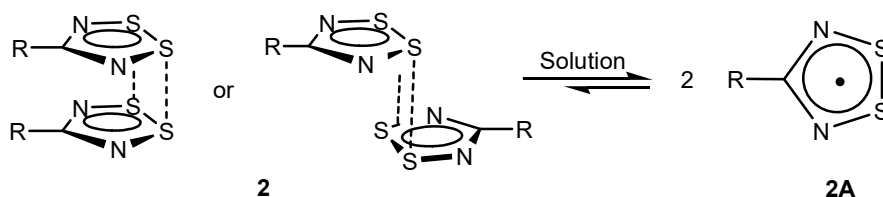
37

38 1. Introduction

39 In the context of our interest in the chemistry of $[\text{CpCr}(\text{CO})_3]_2$ (**1**) with S- and/or P-containing
 40 compounds, we have studied **1**-initiated interchalcogen cleavage in a variety of systems, *viz.* in
 41 homopolynuclear inorganic compounds,¹ in organic substrates, e.g. diphenyldichalcogenides
 42 Ph_2E_2 (E = S, Se, Te),² bis(thiophosphoro)disulfanes, $(\text{R}_2\text{P}(\text{S})\text{S})_2$ (R = Ph^3 and ^iPrO ,⁴
 43 respectively), tetraalkylthiuram disulfanes $(\text{R}_2\text{NC}(\text{S})\text{S})_2$,⁵ dibenzothiazolyl disulfane, ($-\text{S}$
 44 $\text{CSN}(\text{C}_6\text{H}_4)_2$)₂⁶ and dithiobis(tetrazole) $(\text{PhN}_4\text{CS})_2$.⁷ For chalcogen-pnictogen bond cleavage, our
 45 previous work had dealt with the closo polyhedra P_4E_3 (E = S,⁸ Se⁹), the polymeric Sb_2S_3 ,¹⁰ and
 46 Lawesson's reagent.¹¹ The richness of this chemistry is further extended by the homolytic
 47 cleavage of Cr – E bonds (E = N, P, S, Se) in CpCr complexes.¹²

48

49 Scheme 1

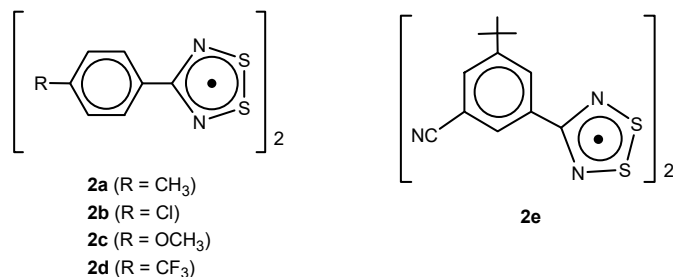


50

51

52 In this present study, we have initiated an investigation of the reaction of **1** with several
 53 substituted aryl 1,2,3,5-dithiadiazolyls, *viz.* (4-R- $\text{C}_6\text{H}_4\text{CN}_2\text{S}_2$)₂, shown in Chart 1 (R = Me, **2a**; Cl,
 54 **2b**; OMe, **2c**; CF_3 , **2d**; $\text{R}^1 = 3\text{-CN}$, $\text{R}^2 = 5\text{-}^t\text{Bu}$, **2e**). The dithiadiazolyls exist in monomer-dimer
 55 equilibrium in solution. (Scheme 1)^{13,14} This class of free radicals, have attracted special
 56 attention in the last few decades,¹⁵ on account of their utility as building blocks for molecular
 57 electronic¹⁶ and magnetic materials^{15d,g} and as chelating ligands for low oxidation state metal
 58 complexes, especially where the ligand remains spin-bearing.¹⁷⁻²⁶ In the present context, their 5-
 59 membered heterocyclic rings present possibilities of C–N, N–S and S–S cleavage reactivity, all
 60 characteristic of the monomeric radical derivative of **1**.^{27,12} In a recent communication^{28a} and
 61 several conference proceedings,^{28b,c} we have reported completely unprecedented π -complexes of
 62 these main-group radicals with **1A**. Here we provide full experimental details for these novel
 63 results and report on their electronic, dynamic NMR and electrochemical properties, including *in*
 64 *situ* EPR spectroelectrochemical studies that identify their radical anions.

65

66 **Chart 1**

68

69 By virtue of the availability of 7π electrons in the ring and a plethora of in-plane electron

70 lone pairs, metal complexes of dithiadiazolyls exhibit variable coordination and ligand-metal

71 bonding.^{24,26} An oxidative addition occurs with zero-valent Pd and Pt phosphine complexes,

72 resulting in S-S bond cleavage and chelation of the resulting disulfide to the metal. With

73 Fe₂(CO)₉ or Fe₃(CO)₁₂,^{17,18} [CpNi(CO)]₂¹⁹ and [Pd(dppe)]₂²² the ring-opened heterocyclic ligand

74 bridges two metal centers in $\mu_2\text{-}\eta^2, \eta^2$ mode as shown in **A-D** in Chart 2, with in **B** and **C** a

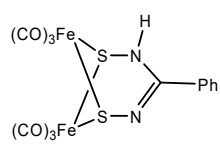
75 retention of paramagnetism, while in **A** and **D** formal hydrogen abstraction by a ligand nitrogen

76 atom occurs to quench paramagnetism. The utilization of two functional ligands leads to

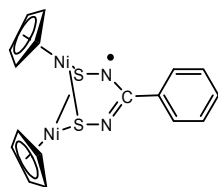
77 trimetallic complexes, **E**. Cooperative binding with N-donor ligands like α -pyridyl, **F**,²⁹ or

78 pyrazine, **G**,³⁰ leads to N,N' chelated complexes that retain the CN₂S₂ unpaired electron.

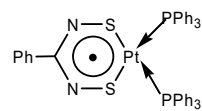
79 **Chart 2**



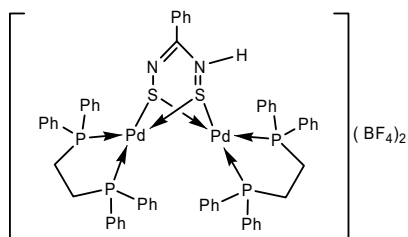
A^{17, 18}



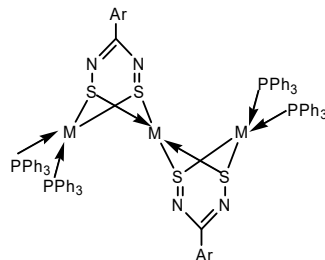
B¹⁹



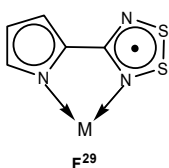
C^{20, 23}



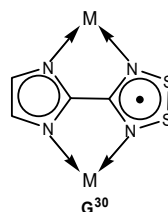
D²²



E a: M = Pt, Pd; Ar = Ph^{20, 23}
b: M = Pd; Ar = 3- & 4-pyridyl²⁵



F²⁹



G³⁰

80

81

82 The formal analogy between thiazyl ring compounds and aromatic or anti-aromatic
83 hydrocarbons has been useful for understanding the diverse chemistry of this class of
84 compounds.¹⁵ In that context, the *absence* of π -complexes to transition metals is particularly
85 noteworthy. A theoretical treatment of η^4 -S₂N₂ coordination was put forward many years ago.³¹
86 However, all known reactions of binary thiazyls such as S₂N₂ and S₄N₄ with metals result either
87 in simple adducts wherein a nitrogen lone pair coordinates to a metal in a stable oxidation state,
88 or by oxidative addition to reactive metals, sometimes with concomitant hydrogen abstraction by
89 a ring nitrogen atom.³² This study is particularly significant for providing the first examples of π -
90 complexes of any thiazyl heterocycles.

91

92 2. Experimental

93

94 2.1 General procedures

95 These were as previously described.^{11a} [CpCr(CO)₃]₂ (1) and Na[CpCr(CO)₃] (1B),³³ and the
96 dithiadiazolyl radicals (2a – 2e)³⁴ were prepared according to literature procedures and the latter
97 were purified by fractional vacuum sublimation.

98

99 **2.2 Reactions of dithiadiazolyls (2a-e) with cyclopentadienylchromium tricarbonyl**
100 **dimer, [CpCr(CO)₃]₂ (1)**

101 The reactions of **2a**, **2b** and **2e** have been described in the Supporting Information of the
102 preliminary communication.^{28a} A typical reaction is described here for **2c**.

103 **CpCr(CO)₂(η^2 -S₂N₂CC₆H₄OMe) (3c)**: (4-OMe-C₆H₄CN₂S₂)₂ (**2c**) (84 mg, 0.20 mmol) and
104 [CpCr(CO)₃]₂ (**1**) (80 mg, 0.20 mmol) were dissolved in toluene (7 mL) and stirred at ambient
105 temperature for 2 h. The resultant reddish-brown reaction mixture was concentrated to dryness
106 and subsequently extracted with n-hexane (10 × 1.5 mL), leaving behind on the walls of the flask
107 a black solid (*ca.* 13 mg, 0.019 mmol, 7.6% yield by weight based on total reactants), which as
108 yet could not be characterized. The reddish-brown extracts were filtered, concentrated to *ca.* 2
109 mL and loaded onto a silica gel column (2 × 10 cm) prepared in n-hexane. Elution gave 3
110 fractions: (i) a green eluate in n-hexane/toluene (3:2, 25 ml), which on concentration gave deep
111 green crystals of [CpCr(CO)₂]₂S (**4**) (*ca.* 15 mg, 0.04 mmol, 20% yield), identified by its color
112 and spectral characteristics (¹H NMR: δ (Cp) 4.36 in benzene-*d*₆ and FAB⁺-MS: *m/z* 378).³⁵ (ii) a
113 red eluate in n-hexane/toluene (1:1, 15 ml), which yielded a red solid of **2c** (*ca.* 16 mg, 0.038
114 mmol, 19% recovery) identified by its EI⁺-MS peak at *m/z* 211 (4-OMe-C₆H₄CN₂S₂) and its
115 fragmentation pattern. (iii) a red eluate in toluene (30 mL), which yielded a fine red crystalline
116 solid of **3c** (*ca.* 110 mg, 0.29 mmol, 72% yield). An immovable green band (*ca.* 2 mm thick) was
117 left uneluted on the column. Anal. for **3c**. Found: C, 46.45; H, 2.87; N, 7.47; S, 16.86. Calc. for
118 CpCr(CO)₂(S₂N₂CC₆H₄OMe): C, 46.87; H, 3.15; N, 7.29; S, 16.68%. ¹H NMR: δ (Cp) 3.86 (s,
119 5H); δ (C₆H₄) 8.15 (br, $\nu_{1/2}$ = *ca.* 15 Hz, 2H); 6.69 (d, 2H) and δ (OCH₃) 3.18 (s, 3H). IR (KBr,
120 cm⁻¹): ν (C=O) 1956vs and 1878vs. FAB⁺-MS: *m/z* 385 [M+1]⁺, 338 [M-2CO]⁺, 195 [CpCrS₂N]⁺.
121 A satisfactory ¹³C NMR data could not be obtained on this product due to sample decomposition
122 in solution.

123

124 **CpCr(CO)₂(η^2 -S₂N₂CC₆H₄CF₃) (3d)**: A similar procedure using **2d** (100 mg, 0.20 mmol) and **1**
125 (80 mg, 0.20 mmol) gave **3d** (*ca.* 62 mg, 0.15 mmol, 37% yield) together with **4** (*ca.* 36 mg, 0.10
126 mmol, 48% yield). Anal. for **3d**. Found: C, 42.70; H, 2.35; N, 6.49; S, 15.16. Calc. for
127 CpCr(CO)₂(S₂N₂CC₆H₄CF₃): C, 42.66; H, 2.15; N, 6.63; S, 15.18%. ¹H NMR: δ (Cp) 3.79 (s, 5H);
128 δ (C₆H₄) 7.99 (br, $\nu_{1/2}$ = *ca.* 14 Hz, 2H) and 7.26 (d, 2H). IR (KBr, cm⁻¹): ν (C=O) 1975vs and

129 1918vs. FAB⁺-MS: m/z 422 [M+1]⁺, 366 [M-2CO]⁺, 195 [CpCrS₂N]⁺. As for **3c**, ¹³C NMR data
130 was not obtained.

131 All the complexes (**3a – 3e**) were found to be air-stable in the solid state. ¹H NMR
132 spectral scans of **3a – 3e** in benzene-*d*₆ showed that all the complexes almost totally converted to
133 Cp₄Cr₄S₄ (**5**) (δ(Cp) 4.91³⁵) after a day at ambient temperature. This instability contributed to our
134 failure to obtain ¹³C NMR data.

135

136 **2.3 Reactions of the dithiadiazolium chlorides (8c, 8d) and S₈ with sodium** 137 **cyclopentadienylchromium tricarbonyl Na[CpCr(CO)₃] (1B)**

138

139 **CpCr(CO)₂(η²-S₂N₂CC₆H₄OMe) (3c):** Na[CpCr(CO)₃] (**1B**) (20 mg, 0.09 mmol) and 4-OMe-
140 C₆H₄CN₂S₂Cl (**8c**) (24 mg, 0.1 mmol) were dissolved in a pre-cooled (-29 °C) solvent mixture of
141 toluene/THF (1:1, 12 mL). The resultant dark red solution was immediately concentrated to *ca.* 2
142 mL, adsorbed onto celite and subsequently evacuated to dryness. A slurry of the celite adsorbate
143 in hexane-toluene (*ca.* 1 mL) was loaded onto a silica gel column (1 x 8 cm) prepared in n-hexane.
144 Elution gave 4 fractions: (i) a green eluate in n-hexane/toluene (3:1, 25 mL), which on
145 concentration gave deep green crystals of [CpCr(CO)₂]₂S (**4**) (*ca.* 9 mg, 0.02 mmol, 53% yield),
146 (ii) a reddish brown eluate in n-hexane/toluene (1:2, 25 mL), which yielded yellow solid 3,7-(4-
147 MeO-C₆H₄)₂{CN₂S₂N₂C} (**7c**) (*ca.* 7 mg, 0.02 mmol, 40%).³⁶ (iii) a red eluate in n-
148 hexane/toluene (1:5, 30 mL), which yielded a fine red crystalline solid of CpCr(CO)₂(η²-
149 S₂N₂CC₆H₄-4-OMe) (**3c**), characterized as above (*ca.* 9 mg, 0.02 mmol, 26% crude yield).
150 Recrystallisation of this in toluene/hexane gave after a day at -29 °C a mixture of red crystals of
151 CpCr(CO)₂(η²-S₂N₂CC₆H₄-4-OMe) (**3c**) (2 mg, 0.005 mmol, 6% yield) and unidentified fine
152 yellow flakes (< 1 mg), from which the red crystals could be physically separated with the aid of
153 a microscope. (iv) a brown eluate in THF, which yielded a 1:1:3 mixture (2 mg) of **4**, **5** and
154 μ²,η²-S₂[CpCr(CO)₂]₂ (**6**), the latter indicated by the presence of δ(Cp) 4.13 in the ¹H NMR
155 spectrum.^{35b,c} An immovable pale blue band (*ca.* 2 mm thick) was left uneluted on the column.
156 During the process of column chromatography, some effervescence (probably of CO) was
157 observed.

158

159 **Data for 7c:** IR (KBr, cm⁻¹): 1604m, 1506m, 1468w, 1440w, 1382s, 1301w, 1252s, 1225m,
160 1168m, 1113w, 1030m, 943w, 840w, 823w, 790w, 730w, 651m, 599w, 524w, 466w; FAB⁺-MS:

161 m/z 358 [M]⁺, 225 [N₃S₂CC₆H₄OCH₃]⁺, 211 [N₂S₂CC₆H₄OCH₃]⁺, 179 [N₂SCC₆H₄OCH₃]⁺, 165
162 [NSCC₆H₄OCH₃]⁺, 150 [NSCC₆H₄OCH₃]⁺, 133 [NCC₆H₄OCH₃]⁺, 103 [NCC₆H₄]⁺; in agreement
163 with literature data.³⁶

164
165 **CpCr(CO)₂(η²-S₂N₂CC₆H₄CF₃) (3d)**: Likewise the reaction of 4-CF₃-C₆H₄CN₂S₂Cl (**8d**) (21
166 mg, 0.07 mmol) with **1B** (16 mg, 0.07 mmol), led to the isolation of **3d** (*ca.* 6 mg, 0.01 mmol,
167 20% yield), along with **4** (*ca.* 23 mg, 0.06 mmol, 24% yield), small amounts of **5** and 3,7-(4-CF₃-
168 C₆H₄)₂{CN₂S₂N₂C} (**7d**) (*ca.* 1 mg, 0.002 mmol, 7%).^{34a} **6** was not observed in this reaction as
169 with the earlier cases. Characterization of **3d** is as given in Section 2.2 above.

170
171 Data for **7d**: IR (KBr, cm⁻¹): ν(C-H) 2928w; ν(other bands) 1612w, 1412w, 1370w, 1317m,
172 1171w, 1135w, 1109w, 1066w, 1015w, 944w, 850w, 685w, 644w, 590w, 529w, 449w; EI-MS:
173 m/z 434 [RCN₂S₂N₂CR⁺, R=CF₃C₆H₄], 263 [RCN₃S₂⁺], 249 [RCN₂S₂⁺], 203 [RCNS], 46 [SN⁺];
174 in agreement with literature data.^{34a}

175 It was found that, at ambient temperature, these reactions gave almost exclusively
176 [CpCr(CO)₂]₂S, a precursor to Cp₄Cr₄S₄, which is the thermodynamic sink for CpCr-thiolato
177 type of complexes.^{1, 12}

178
179 **Reaction with S₈**. A slurry of Na[CpCr(CO)₃] (**1B**) (22 mg, 0.1 mmol) and S₈ (2.2 mg, *ca.* 0.01
180 mmol) in THF was stirred for 5 min and the resultant dark brown solution was subsequently
181 evacuated to dryness. The residue was extracted with toluene (*ca.* 3 x 2 mL), leaving an
182 insoluble dark yellow solid of unreacted **1B**, identified by its ¹H NMR spectrum (δ(Cp) 4.29 in
183 acetone-*d*₆).³⁷ The toluene extract was evacuated to dryness (*ca.* 2 mg) and its ¹H NMR spectra
184 showed 4:2 mixture of [CpCr(CO)₂]₂S (**4**) (7% yield) and μ²,η²-S₂[CpCr(CO)₂]₂ (**6**), (24%),
185 identified by their Cp proton resonances.³⁸

186
187 **2.4 Crystal structure analyses**

188 Diffraction-quality crystals were obtained from solutions in toluene as follows: **3a** as dark
189 red needles after slow evaporation of a concentrated solution for 2 days at ambient temperature,
190 **3b** as dark red hexagons upon layering with ether after 2 days at -29 °C. **3c** and **3d** were obtained
191 as dark red needles from solutions of toluene layered with hexane after 3 days at -29 °C. **3e** as

192 dark red needles upon layering with hexane after 2 days at -29 °C. Crystals of **2d** were grown by
193 vacuum sublimation in a three-zone tube furnace as described previously.³⁹

194 The crystals were mounted on quartz fibers. X-ray data were collected on a Bruker AXS
195 SMART APEX CCD diffractometer (complexes **3a**, **3b**, **3e** and **2d**) or a Siemens SMART
196 diffractometer, equipped with a CCD detector (complexes **3c** and **3d**), using Mo-K α radiation (λ
197 = 0.71073 Å). The data were corrected for Lorentz and polarization effects with the SMART
198 suite of programs⁴⁰ and for adsorption effects with SADABS.⁴¹ Structure solution and refinement
199 were carried out with the SHELXTL suite of programs.⁴² The structure was solved by direct
200 methods to locate the heavy atoms, followed by difference maps for the light, non-hydrogen
201 atoms. The Cp, aryl and alkyl hydrogen atoms were placed in calculated positions. In **3e**, the ^tBu
202 group was found to be disordered; a refinement model using two staggered groups was used for
203 the structure, and the refined occupancies are 60/40. Data collection and processing parameters
204 are given in Table 1. Atom numbering schemes are presented in Figure 2 for **3c,d**; those for
205 **3a,b,e** are as in the preliminary communication.^{28a}

	3a	3b	3c	3d	3e	2d
formula	C ₁₅ H ₁₂ CrN ₂ O 2S ₂	C ₁₄ H ₉ CrClN ₂ O ₂ S ₂	C ₁₅ H ₁₂ CrON ₂ O ₂ S ₂	C ₁₅ H ₉ CrF ₃ N ₂ O 2S ₂	C ₁₉ H ₁₇ CrN ₃ O ₂ S ₂	C ₁₆ H ₈ F ₆ N ₄ S ₄
fw, Daltons	368.39	388.80	384.39	422.36	435.48	498.50
cryst. syst.	triclinic	orthorhombic	monoclinic	monoclinic	triclinic	triclinic
space group	P-1	Pbca	P2 ₁ /n	P2 ₁ /c	P-1	P-1
<i>a</i> , Å	7.7225(9)	13.894(2)	9.8511(6)	9.9853(10)	6.3689(15)	9.4916(9)
<i>b</i> , Å	9.7779(11)	10.9981(15)	7.9608(5)	22.019(2)	12.436(3)	18.1887(17)
<i>c</i> , Å	11.7171(13)	19.653(3)	20.1840(12)	7.3781(8)	12.857(3)	22.275(2)
α, deg	67.524(2)	90	90	90	106.480(5)	91.579(1)
β, deg	86.123(2)	90	100.1910(10)	104.736(3)	91.552(4)	97.329(1)
γ, deg	69.230(2)	90	90	90	92.249(4)	102.755(1)
<i>V</i> , Å ³	762.05(15)	3003.1(7)	1557.91(16)	1568.8(3)	974.9(4)	3713.8(6)
<i>Z</i>	2	8	4	4	2	8
T, K	223(2)	223(2)	223(2)	223(2)	295(2)	173(2)
ρ _{calc} , g cm ⁻³	1.605	1.720	1.639	1.788	1.483	1.783
μ, mm ⁻¹	1.031	1.223	1.017	1.040	0.820	0.583
<i>F</i> (000)	376	1568	784	848	448	2000
θ, deg	1.89-27.50	2.07-27.50	2.05-27.50	1.85-27.50	1.65-25.00	1.85 to 26.22
index ranges	-10 ≤ <i>h</i> ≤ 10 -12 ≤ <i>k</i> ≤ 12 -15 ≤ <i>l</i> ≤ 15	-18 ≤ <i>h</i> ≤ 12 -14 ≤ <i>k</i> ≤ 14 -25 ≤ <i>l</i> ≤ 21	-12 ≤ <i>h</i> ≤ 9 -10 ≤ <i>k</i> ≤ 10 -26 ≤ <i>l</i> ≤ 26	-12 ≤ <i>h</i> ≤ 7 -28 ≤ <i>k</i> ≤ 27 -9 ≤ <i>l</i> ≤ 9	-7 ≤ <i>h</i> ≤ 6 -12 ≤ <i>k</i> ≤ 14 -15 ≤ <i>l</i> ≤ 15	-11 ≤ <i>h</i> ≤ 11 -22 ≤ <i>k</i> ≤ 22 -27 ≤ <i>l</i> ≤ 27
reflns collect.	10001	19853	10776	11106	5146	39140
unique reflns	3489	3441	3582	3590	3418	14828
data/ restr./ param.	3489/0/200	3441/0/199	3582/0/209	3590/0/226	3418/18/259	14828/18/1089
<i>R</i> indices (<i>I</i> > 2σ(<i>I</i>)) ^{a,b}	R1 = 0.0511 wR2 = 0.1093	R1 = 0.0726 wR2 = 0.1437	R1 = 0.0414 wR2 = 0.0955	R1 = 0.0689 wR2 = 0.1345	R1 = 0.0703 wR2 = 0.1446	R1 = 0.0568 wR2 = 0.1005
<i>R</i> indices (all data)	R1 = 0.0617 wR2 = 0.1139	R1 = 0.0867 wR2 = 0.1490	R1 = 0.0508 wR2 = 0.1002	R1 = 0.0883 wR2 = 0.1414	R1 = 0.1359 wR2 = 0.1690	R1 = 0.1431 wR2 = 0.1272
GOF on <i>F</i> ^{2c}	1.159	1.300	1.072	1.213	0.940	0.990
largest peak, hole, e Å ⁻³	0.548, -0.411	0.794, -0.622	0.369, -0.260	0.524, -0.507	0.476, -0.278	0.812, -1.013

208 ^a R1 = (Σ|*F*₀ - |*F*_c||Σ|*F*₀).209 ^b wR2 = ((Σw|*F*₀ - |*F*_c||²/Σw|*F*₀|²)^{1/2}.210 ^c GOF = ((Σw|*F*₀ - |*F*_c||²/(N_{observns} - N_{params}))^{1/2}.

211

2.5 Electrochemistry and SEPR spectroscopy

Voltammetric experiments were conducted with a computer controlled Eco Chemie μ Autolab III potentiostat with 1 mm diameter glassy carbon (GC) and Pt working electrodes. Potentials were referenced to the ferrocene/ferrocenium (Fc/Fc⁺) redox couple, which was used as an internal standard. The electrochemical cell was thermostated at 233 and 293 K using an Eyela PSL-1000 variable temperature cooling bath.

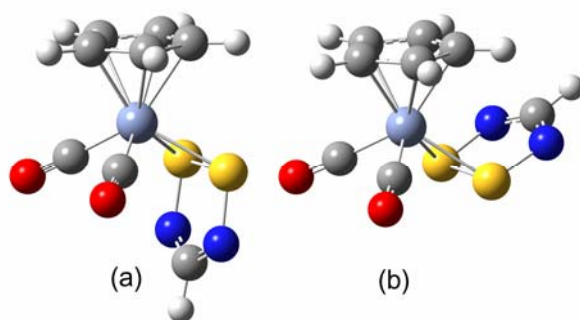
Simultaneous electrochemical electron paramagnetic resonance (SEPR) spectroscopy experiments were conducted in conventional EPR flat cells in a Bruker TE₁₀₂ cavity using a modified version of a cell described in the literature based on an Au-micromesh working electrode.⁴³ The spectrometer was an EMX113/12 model operating in X-band (9.4 GHz) under ambient conditions or at reduced T employing the standard Bruker LN₂ cryostat and a miniature EPR flat cell.⁴⁴ Solutions of the complex (conc. for **3a** 8.0 mM; **3b**, 1.7 mM, **3c**, 8.7 mM; **3d**, 3.6 mM; **3e** 4.6 mM) in CH₃CN containing 0.1 M ⁿBu₄NPF₆ were loaded into the flat cell (ca. 2 mL), and background EPR spectra were obtained. Subsequently cyclic voltammograms were obtained *in situ*, and the potential adjusted to the anodic (oxidation) or cathodic (reduction) peak potentials. Single scans of 40s or 80s were obtained simultaneous with electrolyses of the same duration. Radical lifetimes were determined by setting the EPR field at the signal center and scanning in the time dimension, first setting a baseline, then commencing electrolysis until maximum signal intensity was obtained, stopping electrolysis and monitoring the decay of the signal. First-order decay curves were fitted to exponential decay (correlation coefficient ≥ 0.99). The reported EPR parameters were obtained from complete digital line-fitting routines using WinSim 2002.⁴⁵

2.6 Hybrid DFT Calculations

The structures of diamagnetic adducts η^5 -CpCr(CO)₂(η^2 -S₂N₂CH) in *exo*, **3f**, and *endo*, **3g**, conformations were optimized with C_s symmetry in their ground states using density functional theory in the GAUSSIAN 98W suite of programs.⁴⁶ The B3PW91 functional⁴⁷ with the 1991 gradient-corrected correlation functional of Perdew and Wang⁴⁸ was used; this hybrid functional has previously been shown to provide realistic geometries for organochromium complexes.⁴⁹ The Gaussian basis set 6-31+G(d) was used for geometry optimization and 6-311+G(2d,2p) for the final energy calculations. The computed structures are illustrated in Figure 1, while Table 2

243 includes the calculated bond distances and angles. A more complete list of geometrical
244 parameters is shown in Figure S6.

245



247

248 **Figure 1.** Optimized model complexes of (a) *exo* isomer **2f** (-2409.1423602 Hartree) and (b)
249 *endo* isomer **2g** (-2409.143318 Hartree) from B3PW91/6-311+G(2d,2p)//B3PW91/6-31G(d)
250 calculations. Atom codes: Cr, light blue; S, yellow; N, dark blue; O, red; C, gray; H, white. Bond
251 distances and angles for these structures are included in Table 2.

252

253 2.7 Dynamic NMR experiments

254 The ^1H spectra obtained from 200 to 300 K were subjected to lineshape analysis using both the
255 Cp and aromatic signals. The Cp signal was treated as a two-site, one-spin- $\frac{1}{2}$, unequally
256 populated, exchange system including transverse relaxation for both sites. Spectra were
257 simulated using an implementation of the McConnell⁵⁰ formalism in Matlab.⁵¹ In this approach
258 the Bloch equations are modified to include chemical exchange but do not include weak coupling
259 effects. The aromatic region was treated as an unequally populated two-site four-spin system.
260 This system was treated using a time dependent quantum mechanics approach utilizing the
261 density matrix.⁵² The aromatic spin systems on both sites were assumed to be AA'BB'. This
262 density matrix treatment was also implemented in Matlab. Both analyses used chemical shifts,
263 scalar couplings, transverse relaxation times as input parameters for each nucleus along with the
264 equilibrium constant and exchange rate.

265 For each temperature, candidate spectra were computed for particular chemical shifts,
266 scalar couplings, relaxation times, equilibrium constants and the rate constants, and these were
267 compared visually with the experimental traces. The rate constant was changed until an optimal
268 match was achieved. Values for the equilibrium constant, chemical shift and relaxation times
269 were obtained by extrapolating measurements from the lower temperatures where chemical

270 exchange effects do not interfere with the measurements. In this manner, determinate error due to
271 temperature drift in these parameter can be removed, greatly increasing the accuracy of the rate
272 measurements.⁵³ Errors in the rate measurements were estimated by perturbing the rate until
273 differences with the experimental spectrum became apparent. We estimate that rate
274 measurements accurate to within 10% are achieved.⁵³ The activation parameters for each data set
275 were determined from the rate measurements using the Eyring equation. The activation enthalpy
276 was obtained from the slope and the activation entropy from the intercept.^{54,55} Similarly the
277 enthalpy and entropy difference between the two isomers was obtained from the equilibrium
278 constants using the temperature dependence of the Gibbs energy. A complete set of the spectral
279 changes and line-fits are provided in Figures S1-3. The original equilibrium and rate data as well
280 as the Eyring plots are provided in Tables S1-S2 and Figures S4-S5. Summary data extracted
281 from the fits is presented in Table S3.

282

283 **3 Results and Discussion**

284

285 **3.1 Reaction of cyclopentadienylchromium tricarbonyl dimer, [CpCr(CO)₃]₂ (**1**) with** 286 **1,2,3,5-dithiadiazolyl dimers in equimolar ratios**

287 The reactions of [CpCr(CO)₃]₂ (**1**) with 1 mol equiv of (4-R-C₆H₄CN₂S₂)₂ (R = Me, **2a**; Cl, **2b**;
288 OMe, **2c**; CF₃, **2d**; 3-CN, 5-^tBu, **2e**) in toluene at ambient temperature led to the isolation of
289 deep-green crystals of [CpCr(CO)₂]₂S (**4**) and fine red crystalline solids of CpCr(CO)₂(η²-
290 S₂N₂CC₆H₄R) (R = 4-Me, **3a**; 4-Cl, **3b**; 4-OMe, **3c**; 4-CF₃, **3d**) and CpCr(CO)₂(η²-S₂N₂CC₆H₃-3-
291 (CN)-5-^tBu)) (**3e**) in yields shown in Scheme 2.

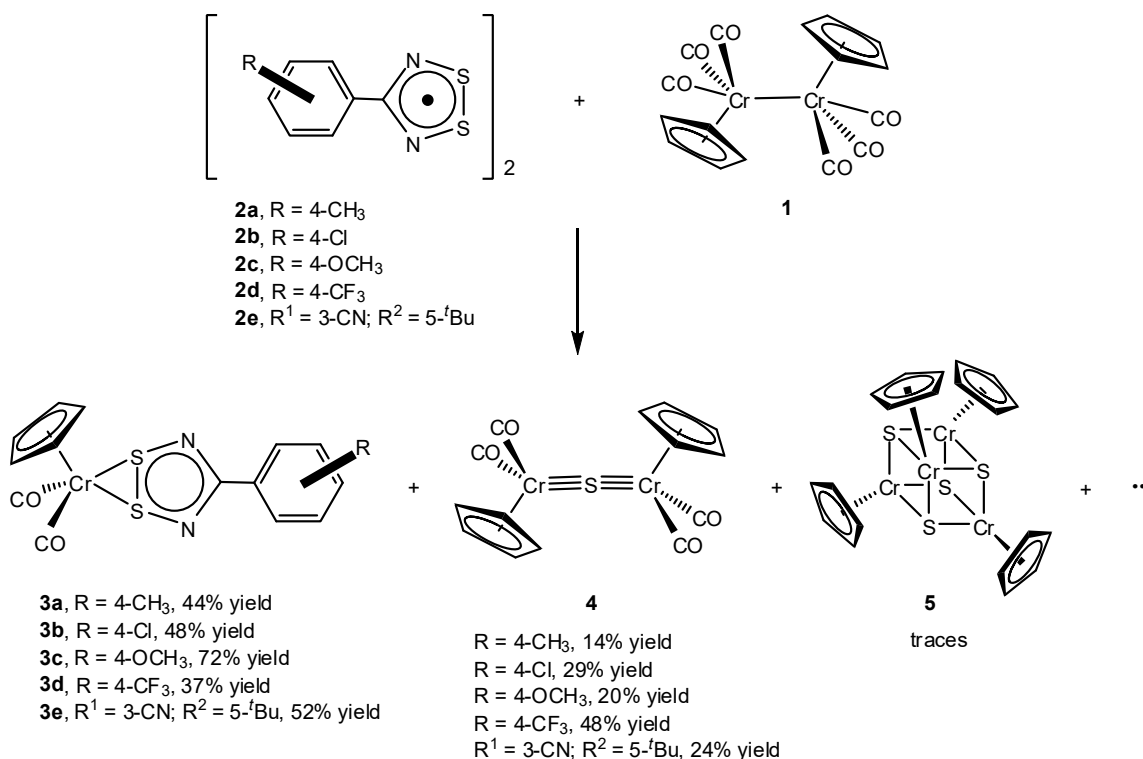
292 ¹H NMR tube reactions showed that (i) using 2 mole equivalents of **1** to **2** gave higher
293 yields of **4**, together with two other unidentifiable by-products possessing δ(Cp's) 4.48 and 4.51,
294 with relative molar ratio being, respectively 14 : 1 : 2 : 10 (for **3a**). (ii) **3a** reacted readily with
295 one mole equivalent of **1** at ambient temperature, undergoing 25% conversion to **4** after 2.5 h. (iii)
296 with 2 mole equivalents of **1**, **3a** was more than 90% transformed after a day to **4**, **5**, and the
297 unknowns 'δ 4.48' and 'δ 4.51' in relative molar proportion of 200 : 5 : 1 : 7. These NMR
298 experiments confirm that a most probable route to **4** is the interaction of the primary product **3a**
299 or **3b** with excess of **1**, resulting in S-abstraction from the coordinated heterocyclic ring of
300 dithiadiazolyls. Indeed, our previous work had demonstrated the role of **1A** as a strong thiophile,
301 capable of abstracting S from various classes of S-containing ligands at a CpCr center, leading to

302 partially or fully *desulfurized* derivatives.^{7,12} Unfortunately in this particular case, we were
 303 unable to isolate the resulting metal complex or organic products, nor obtain any clear indication
 304 of their presence in NMR spectral analysis of the solution of total crude products.

305

306 **Scheme 2**

307



308

309

310 **3.2 Reaction of sodium cyclopentadienylchromium tricarbonyl, Na[CpCr(CO)₃] (**1B**) with**
 311 **1,2,3,5-dithiadiazolium chlorides**

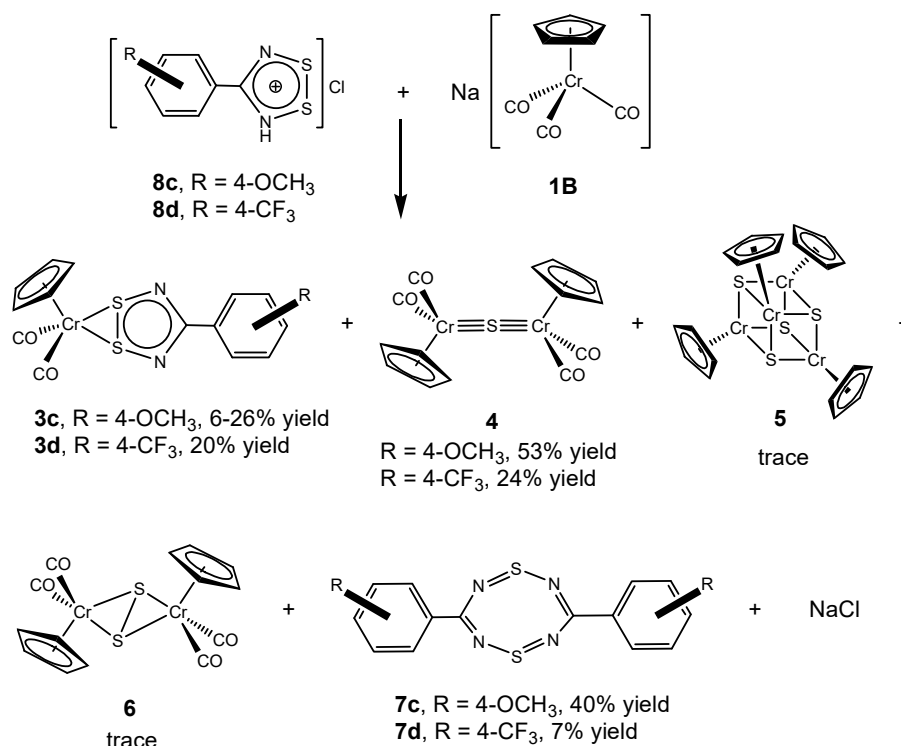
312

313 The very rapid reactions of Na[CpCr(CO)₃] (**1B**) with 1 mol equiv of 4-R-C₆H₄CN₂S₂Cl (R =
 314 OMe, **8c**; CF₃, **8d**) in toluene/THF at -29 °C led to the isolation of 3,7-(4-R-C₆H₄)₂{CN₂S₂N₂C}
 315 (R = OMe, **7c**, 40%; CF₃, **7d**, 7%) and fine red crystalline solids of CpCr(CO)₂(η²S₂N₂CC₆H₄R)
 316 (R = OMe, **3c**, 6%; CF₃, **3d**, 20%), along with **4**, **5**, **6** and NaCl shown in Scheme 3. The lower
 317 yields of **3c** and **3d** here obtained as compared with those from the radical reactions were
 318 unexpected, as higher yields were anticipated from this direct metathetic salt elimination reaction.
 319 This observation may be ascribed to the high thermal instability of the complexes **3c**, which
 320 readily transforms to **5** via **4**. Indeed, in an NMR tube study, complex **3c** could only be detected

321 in the product mixture from a reaction at $-30\text{ }^{\circ}\text{C}$; at ambient temperature **4** was the predominant
 322 product. It may be plausible that the exothermic heat of formation of NaCl in the ‘salt’ reaction
 323 contributed to the degradation of complexes **3**. However, though this may be substantiated by a
 324 comparison of the relative yield of **4:3c** in the radical and salt reactions, the same inference
 325 cannot be drawn in the case of **3d**, wherein the **4:3d** yield ratio remains relatively unchanged in
 326 both types of reactions.

327

328 **Scheme 3**



329

330

331

332 A more likely mechanism would involve a prior redox reaction between $[\text{CpCr}(\text{CO})_3]^-$
 333 (**1B**) and $[\text{RC}_6\text{H}_4\text{CN}_2\text{S}_2]^+$ (**8c-d**), generating the radical species, $\text{CpCr}(\text{CO})_3^\bullet$ (**1A**) and
 334 $\text{RC}_6\text{H}_4\text{CN}_2\text{S}_2^\bullet$ (**2A**), which then couple to form **3**, as in the reaction between the dimeric species.
 335 This postulate is supported by electrochemical data, which shows that these two systems are
 336 ‘redox-incompatible’,⁵⁶ the redox potentials, ($E_{1/2}$) vs. SCE being +0.57 V (**8c**, R = 4-OMe) and
 337 +0.66 V (**8d**, R = 4-CF₃) for $[\text{RC}_6\text{H}_4\text{CN}_2\text{S}_2]^{+/\bullet}$ ⁵⁷ and -0.28 V for $[\text{CpCr}(\text{CO})_3]^{-/\bullet}$.⁵⁸ Thus the
 338 strongly oxidizing property of **8c-d** in concert with the strongly reducing property of **1B** provides
 339 the driving force for a redox reaction which generates the corresponding radical precursors **2A**

340 and **1A** to complexes **3**.⁵⁶ Support for the above postulate is provided by the isolation of the
341 dithiatetrazocines **7c-d**, which are known oxidation products of the free radicals.^{34a} Structurally it
342 is evident that these arise from coupling of the desulfurized derivative $\text{RC}_6\text{H}_4\text{CN}_2\text{S}^*$ of **2A**, which
343 by inference and *inter alia* must have been present in this ‘salt’ reaction. Based on our
344 observation of the sluggish reaction of **1B** with S_8 to give **4** in 7% yield versus the facile
345 quantitative yield in analogous reaction of **1/1A**,^{385b,c} the obtained high yields of **4** in this reaction
346 (53 and 24 %) also argues against the anion **1B** being the active reagent, and supports the
347 intermediary role of the radical **1A**.

348

349 **3.3 Crystal structure and spectroscopic analyses**

350 The molecular structures of these complexes show that the coordination geometry at Cr is
351 similar, with Cr atoms assuming a four-legged piano-stool configuration, being bonded to a
352 bidentate (S,S) dithiadiazolyl ligand and two CO ligands. However, the relative orientations of
353 the heterocyclic ligands are very different. The dithiadiazolyl ligand of **3a** and **3d** is orientated
354 towards the CO ligands, away from the Cp ring (*exo* configuration), while that of **3b**, **3c** and **3e**
355 is orientated away from the CO ligands, and towards the Cp ring (*endo* configuration). The hinge
356 angles at the S—S bonds between the CrS_2 and S_2N_2 planes are $+65.2^\circ$ in **3a**, -65.7° in **3b**,
357 -66.5° in **3c**, $+63.6^\circ$ in **3d** and -67.2° in **3e**. Torsion angles between the S_2N_2 and aryl rings
358 vary from $3 - 16^\circ$. The molecular structures for an *endo* isomer (**3c**) and an *exo* isomer (**3d**) are
359 depicted in Figure 2. Selected metric data of all five structures are given in Table 2.

360

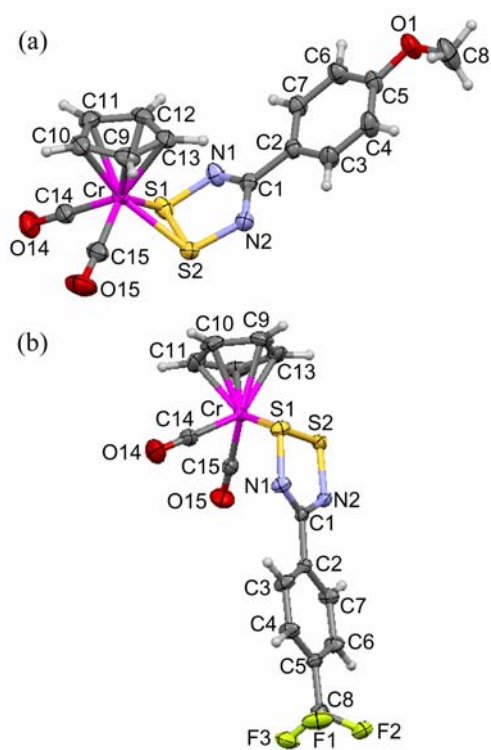


Figure 2. Thermal ellipsoid plots showing the molecular structures of (a) *endo* **3c** and (b) *exo* **3d** as found in the crystals.

Table 2. Metric data from crystallography and DFT calculation

Compound:	3a ^a	3b ^a	3c ^a	3d ^a	3e ^a	3f ^b	3g ^b
Isomer:	<i>exo</i>	<i>endo</i>	<i>endo</i>	<i>exo</i>	<i>endo</i>	<i>exo</i>	<i>endo</i>
Bond Distance (Å)							
Cr(1)-S(2)	2.3454(9)	2.3537(12)	2.3407(7)	2.3505(12)	2.361(2)	2.3721	2.3878
Cr(1)-S(1)	2.3463(9)	2.3602(13)	2.3688(7)	2.3334(12)	2.3540(19)	2.3721	2.3878
S(1)-N(1)	1.640(3)	1.642(4)	1.640(2)	1.642(4)	1.636(5)	1.6478	1.6542
S(1)-S(2)	2.1143(10)	2.1315(15)	2.1487(9)	2.1280(15)	2.146(3)	2.2108	2.2021
S(2)-N(2)	1.644(2)	1.635(4)	1.641(2)	1.627(3)	1.632(5)	1.6478	1.6542
N(1)-C(1)	1.340(4)	1.337(5)	1.333(3)	1.330(5)	1.335(7)	1.3301	1.3290
N(2)-C(1)	1.332(4)	1.333(6)	1.338(3)	1.340(5)	1.329(8)	1.3301	1.3290

Bond Angle (°)							
S(2)-Cr(1)-S(1)	53.57(3)	53.77(4)	54.29(2)	54.04(4)	54.14(7)	55.55	55.04
N(1)-S(1)-S(2)	94.77(9)	93.79(13)	93.31(8)	93.48(13)	93.3(2)	92.63	92.77
N(1)-S(1)-Cr(1)	114.76(10)	112.62(14)	111.87(8)	114.91(13)	110.99(19)	112.99	112.81
S(2)-S(1)-Cr(1)	63.19(3)	62.96(4)	62.19(2)	63.39(4)	63.10(7)	62.22	62.48
N(2)-S(2)-S(1)	93.62(9)	93.79(14)	93.53(8)	94.35(13)	93.5(2)	92.63	92.77
N(2)-S(2)-Cr(1)	113.17(9)	114.00(14)	113.08(7)	115.49(13)	112.6(2)	112.99	112.81
S(1)-S(2)-Cr(1)	63.24(3)	63.27(4)	63.52(2)	62.57(4)	62.76(7)	62.22	62.48
C(1)-N(1)-S(1)	113.3(2)	114.2(3)	114.88(17)	114.3(3)	114.5(4)	114.23	114.22
C(1)-N(2)-S(2)	114.3(2)	114.6(3)	114.39(17)	114.0(3)	114.5(4)	114.23	114.22

369 ^a Full geometrical details are provided in the *CIF* files.

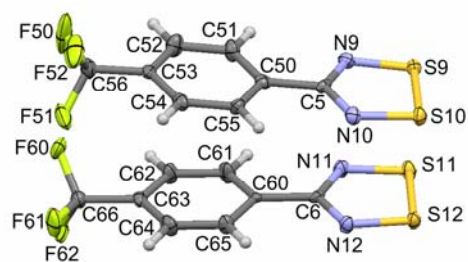
370 ^b From B3PW91/6-311+G(2d,2p)// B3PW91/6-31G(d) calculations within C_{2v} symmetry.

371

372

373 While there are many reported structures for dithiadiazolylys in the literature, of those
 374 employed here, only **2c**⁵⁹ and **2e**^{34b} have been reported previously. We report the structure of **2d**
 375 for the first time. While many dithiadiazolylys undergo phase transitions on cooling that affect
 376 crystallinity, we were able to obtain a structure for **2d** at 173 K. A typical *cis*-cofacial²⁶ dimer
 377 structure is displayed in Figure 3.⁶⁰ The molecule shows evidence of distortion to accommodate
 378 the bulky *para* CF₃ groups, so that *e.g.* the two inter-annular S...S contacts are quite dissimilar.
 379 The association of dithiadiazolylys in this fashion has been convincingly attributed to diffuse
 380 $\pi^*-\pi^*$ interactions between the two ring SOMOs,⁶¹ as indicated by inter-annular S...S distances
 381 considerably longer than the Cr-S distances in **3** (see below.)

382



383

384 **Figure 3.** Thermal ellipsoids plot of one of the four *cis*-cofacial dimers found in the crystal
385 structure of **2d**. In this particular dimer $d(\text{S9}\cdots\text{S11}) = 3.054 \text{ \AA}$ and $d(\text{S10}\cdots\text{S12}) = 3.031 \text{ \AA}$. The
386 average $d(\text{S—S}) = 2.083(5) \text{ \AA}$, $d(\text{S—N}) = 1.629(7) \text{ \AA}$ and $d(\text{N—C}) = 1.337(4) \text{ \AA}$ over all eight
387 monomers (errors are standard deviations).

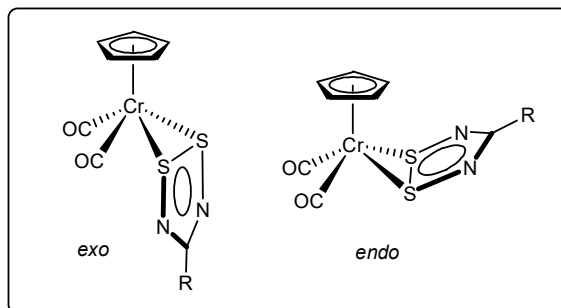
388
389 In the metal complexes, the CN_2S_2 ring of the heterocyclic ligand remains intact, with
390 only some lengthening (*ca.* 2%) of the S—S bond upon coordination ($2.1143(10) \text{ \AA}$ in **3a**,
391 $2.1315(15) \text{ \AA}$ in **3b** versus $2.103(5) \text{ \AA}$ in unligated **2b** at RT,⁵⁹ $2.1487(9) \text{ \AA}$ in **3c**, $2.1280(15) \text{ \AA}$
392 in **3d** versus an average $2.083(5) \text{ \AA}$ over eight unique molecules of **2b** at 173K and $2.146(3) \text{ \AA}$ in
393 **3e** versus $2.101(2) \text{ \AA}$ in **2e**),^{34b} while the C—N and S—N bonds remain virtually unchanged (*ca.*
394 $1.330\text{--}1.340$ and $1.627\text{--}1.644 \text{ \AA}$, respectively, versus $1.337(4)$ and $1.629(7) \text{ \AA}$ in the free ligand
395 **2d**, for instance). There thus exists a strained three-membered CrS_2 ring, with a small S—Cr—S
396 bond angle ($53.57(3)^\circ$ in **3a** - $54.29(2)^\circ$ in **3c**). These angles are larger than those in
397 $\text{Cp}_2\text{Cr}_2(\text{CO})_4(\mu\text{-}\eta^2\text{-S}_2)$ ($48.8(0)$ and $49.0(0)^\circ$) and in $\text{Cp}_2\text{Cr}_2(\text{CO})_5(\mu\text{-}\eta^1, \eta^2\text{-S}_2)$ ($50.1(1)^\circ$), which
398 undoubtedly are related to the shorter S—S bonds of $1.990(1)$ and $2.010(4) \text{ \AA}$, respectively,^{38c}
399 but they are, as expected, smaller than the ‘open’ S—Cr—S angles ($70.3\text{--}83.65^\circ$) found in
400 $\text{CpCr}(\text{CO})_2$ complexes containing bidentate S_2PPh_2 ,³ $\text{S}_2\text{P}(\text{O}^i\text{Pr})_2$,⁴ S_2CNR_2 ^{5b} and $\text{S}_2\text{CO}^i\text{Pr}$
401 ligands.⁶² The Cr—S bond lengths (range $2.3334(12) - 2.3688(7) \text{ \AA}$) lie at the low end of the range
402 previously observed for other CpCr complexes, *viz.* $2.348(2)\text{--}2.466(2) \text{ \AA}$ for complexes
403 containing bare S ligands,^{38c} $2.321(4)\text{--}2.517(3) \text{ \AA}$ for complexes containing bare P/S ligands,⁸
404 $2.365(1)\text{--}2.471(3) \text{ \AA}$ for complexes containing bridging SPh ligands,^{2a} and $2.3711(8)\text{--}2.517(8)$
405 \AA for complexes containing S_2PR_2 or $\text{S}_2\text{P}(\text{OR})_2$.³⁻⁴

406 The bonding mode in **3a-e** is new for dithiadiazolyl metal chemistry. To date transition
407 metal complexes or their fragments have always cleaved the S—S bond of the heterocyclic ring
408 (see examples in Chart 2). In these cases the reported S \cdots S distances fall between 2.91 and 3.17
409 \AA ,¹⁹⁻²⁶ consistent with almost zero bond order according to the estimated values of 2.03 and 1.60
410 \AA for the effective radii of sulfur, perpendicular to and along the bond.⁶³

411 Considering the formal uni-negative charges of the Cp and dithiadiazolyl ligands⁶⁴ and
412 the overall neutrality of the complexes, the Cr centers can be considered to be in +2 oxidation
413 state. With the heterocyclic ligand as a 3-electron donor, the 18-electron rule is obeyed in each of

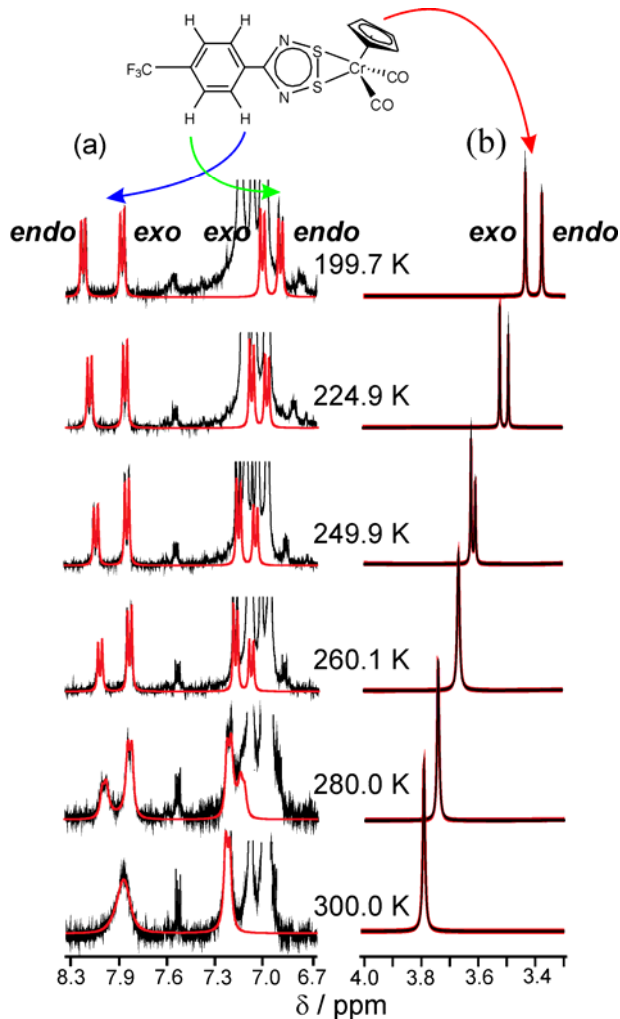
414 the complexes and this is reflected in their predominantly diamagnetic nature as indicated in their
415 proton NMR spectra.

416 The molecular structures of these complexes are supported by their IR, NMR and mass
417 spectral data. The IR spectra possess two terminal CO stretches. The ^1H -NMR spectra show for
418 **3a** $\delta(\text{Cp})$ 3.86 and $\delta(\text{Me})$ 2.00, for **3b** $\delta(\text{Cp})$ 3.80, for **3c** $\delta(\text{Cp})$ 3.86 and $\delta(\text{OMe})$ 3.18, for **3d**
419 $\delta(\text{Cp})$ 3.79, and for **3e** $\delta(\text{Cp})$ 3.78, together with broad unresolved multiplets for the arene
420 protons in all cases. The parent ions $[\text{M}+1]^+$ are seen in their FAB^+ -mass spectra.



421
422 **3.4 Dynamic ^1H NMR study of **3d****
423 The discovery of *endo* and *exo* conformations in different derivatives of **3** in the solid
424 state caused us to examine their solution ^1H NMR spectra carefully; in each case only one set of
425 signals due to **3** occurs in RT spectra in d_6 -benzene (see Experimental), with the expected singlet
426 from Cp and two aromatic AA' and BB' doublets for **3a-d** and three distinct aromatic peaks for
427 **3e**. However, for each compound at least one of the aromatic signals was line-broadened at RT
428 indicative of dynamic processes in solution. Therefore we carried out a variable temperature ^1H
429 NMR experiment in d_8 -toluene on the most soluble exemplar available to us, complex **3d** (an *exo*
430 isomer in the crystal). On cooling, complex spectral changes occur in this system (Figures 4 and
431 S1).

432

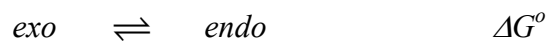


433
 434 **Figure 4.** Stacked plots of ^1H NMR traces in (a) the AA'BB' aromatic and (b) the Cp regions of
 435 **3d** over the range 200 – 300 K, showing every second temperature measured. Experimental data
 436 in black; computed spectra from line-shape fitting in red. Unfitted lines are either due to the
 437 residual d_8 -toluene signals or minor impurities; the aromatic region has a much increased vertical
 438 scale, the more so at high temperature where coalescence broadening occurs. The RMS noise in
 439 the baseline of part (a) and (b) are identical; the vertical scale in (a) is greatly enlarged.

440
 441 Both the aromatic and Cp signals separate at different temperatures into two sets of
 442 signals. The population of the two interchanging species is strongly temperature dependent ($K =$
 443 $[\textit{endo}]/[\textit{exo}]$ ranges from ~ 0.6 at RT to ~ 0.9 at 200 K), and their chemical shifts are also strongly
 444 temperature dependent (thus *average* $\delta(\text{Cp})$ moves 0.37 ppm to higher field; *average* $\delta(\text{AA}')$
 445 aromatic set by 0.13 and $\delta(\text{BB}')$ by 0.10 ppm to lower field on cooling from RT to 200K).

446 First, we attempt to assign the spectra. From considerable experience with disubstituted
447 aryl groups attached to thiazyl rings, we can confidently assign the broad aryl ^1H resonance at $\sim\delta$
448 8.0 ($\nu_{1/2} = 14$ Hz) in the RT spectrum to the benzene hydrogen atoms *ortho* to the CN_2S_2 ring,
449 and hence the δ (7.25) set to the *meta* atoms. For example, in **3e** the two broadened signals occur
450 at δ 8.36 and 8.16. We note that the lower-population isomer at 200 K displays its Cp resonance
451 0.11 ppm to *higher* field of the higher-intensity signal, and its AA' aromatic signals 0.5 ppm to
452 *lower* field of the other AA' signal, with a smaller but opposite shift for BB'. We think the most
453 likely cause of these differential shifts is the presence of ring-current effects in the *endo* isomer
454 which are largely absent in the *exo* isomer. On the assumption that the aryl— CN_2S_2 bond is in
455 rapid rotational exchange, the aryl protons will experience in-plane shielding from the aromatic
456 Cp ring, an effect that is expected to operate on the *ortho* hydrogens, whereas the *meta*
457 experience weak anisotropic shielding as a consequence of geometry. Additionally, the Cp H
458 atoms will experience strong out of plane shielding from the aromatic CN_2S_2 rings in these
459 complexes. Hence we assign the most shielded Cp and most de-shielded signals to the *endo*
460 isomer, the species with the lower population in solution. The dynamic nature of all these signals
461 makes confirmation of the assignment by NOESY unfeasible.

462 Complete line fitting was performed on both the Cp and AA'BB' aryl regions of the ^1H
463 NMR spectrum of **3d** over the range 200 – 300 K (Figure 4). From the integration of the signals
464 due to the two isomers we have measured the equilibrium constants, and hence rates, for the
465 process:



467
468 and from the inverse $\log K$ vs. $1/T$ plots extracted ΔH° and ΔS° . From an average of the
469 analyses from the two spectral regions we obtain $\Delta H^\circ = -3 \pm 1$ kJ mol $^{-1}$ and $\Delta S^\circ = -15 \pm 1$ J K $^{-1}$
470 mol $^{-1}$, indicating that the preference for *exo* above 190 K is entropically driven and that the *endo*
471 isomer is enthalpically slightly more stable.

472 Of greater interest are the activation parameters for the conversion of the two isomers.
473 The linewidth data were available over a relatively small temperature range, imposed by solvent
474 melting point and the analyte's thermal stability. Moreover, dynamic effects on the lineshapes
475 occur in this system over only about a 40 K range. As a result, it was not possible to obtain
476 uncorrelated ΔH^\ddagger and ΔS^\ddagger values, so that only the free energy of activation can be reported.

477 There is good agreement in ΔG^\ddagger between the analyses on the Cp and aromatic signals, with
478 $\Delta G_{298}^\ddagger = 59 \pm 4$ kJ mol⁻¹. The statistical analysis for the data from the Cp signals indicates a much
479 smaller error in this parameter (see Table S3 for the original data); however, from previous
480 experience the error in ΔH^\ddagger is typically ± 1 kJ mol⁻¹ and in $\Delta S^\ddagger \pm 5$ J K⁻¹ mol⁻¹.⁵⁵ At 298 K these
481 errors would predict an error of 1.8 kJ mol⁻¹ in ΔG^\ddagger , about half of the variance we observe
482 among the two data sets.

483 We now consider possible mechanisms for *exo/endo* conversion. Among various
484 conceivable intra-molecular processes a variant on the classic organometallic “ring-whizzing”
485 mechanism, in which there is rotation about the centroid of the S—S bond, shows a much lower
486 barrier than a “hinge” mechanism which flips the ligand ring about a stationary S—S bond,
487 according to semi-empirical PM3-TM calculations. However, *exo/endo* exchange may also be
488 dissociative, a notion that accords well with the intrinsic stability of both radicals **1A** and **2A**.
489 The strong temperature dependence of the Cp and *meta* aromatic proton chemical shifts does
490 suggest the presence of small but increasing amounts of a paramagnetic species with a rise in
491 temperature. These shift effects are reversible and – if due to dissociation – the amount of
492 paramagnetic species remains small and in fast exchange at all temperatures, which suggests a
493 very small barrier but a large ΔH° . (EPR studies, see below, support the notion that the amount
494 of dissociation is very small). Hence these limited data suggest that both an intra-molecular
495 process (e.g. ring-whizzing), with an appreciable barrier but small enthalpy difference, and
496 dissociation, with a very low barrier but a large enthalpy difference, operate simultaneously. The
497 DNMR results thus support the notion that **3d** exists as *endo* and *exo* isomers in solution, with
498 the *exo* configuration thermodynamically favored at RT, but with the *endo* having the lower
499 internal energy. We believe similar effects operate for **3a-e** and attribute the distribution of
500 isomers in the crystal structures that we obtained to either crystal packing forces favoring a given
501 isomer or to fortuitous crystal picking from among a mixture.

502

503 **3.5 Structure and Bonding – Hybrid DFT calculations and comparison to allyl complexes**

504

505 Both calculation and the crystallographic measurements seem to indicate a distinct difference in
506 bond lengths between the *exo* and *endo* isomers within the CrS₂N₂C coordinated rings. Averaged
507 bond distances over the five crystal structures are compiled in Table 3 for ease of comparison
508 with the B3PW91/6-31G(d) calculated values. The errors reported here are root-mean-square

509 values of the individual values from the crystallographic least squares refinements. The average
 510 Cr—S and S—S distances are both shorter in the *exo* isomers within these experimental errors,
 511 although the difference is less than one percent. On the other hand, the S—N and N—C distances
 512 are not distinguishable within experimental errors. The DFT-calculated values differ by similar
 513 amounts between the two isomers, but most of the computed distances are longer than the
 514 measured values by more than the difference between isomers. Curiously, the *endo* isomer **3g** is
 515 calculated to be more stable than the *exo* isomer **3f** by 2.5 kJ/mol in the gas phase at the
 516 B3PW91/6-311+G(2d,2p)//B3PW91/6-31G(d) level of theory, possibly because other bond
 517 lengths in the molecule are stabilized in **3g** sufficiently to compensate for the longer distances
 518 within the CrS₂N₂C moiety. This difference in stability is, however, small in comparison to well-
 519 documented limitations on the accuracy of the theoretical methods employed. Thus, while DFT
 520 cannot distinguish reliably between the stability of the two isomers, the solution-phase NMR
 521 data for **3d** also support the notion that the *endo* isomer is the enthalpically more stable, at least
 522 insofar as the NMR assignment is correct. The important point is that both isomers are entirely
 523 feasible and apparently bind to the Cr atom with very similar bond types and bond energies.

524

525 **Table 3.** Average Bond Distances compared to DFT calculations

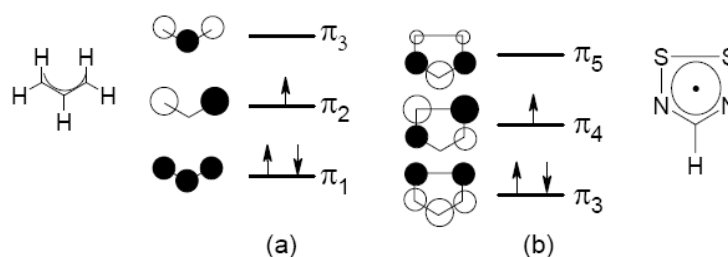
Bond Distance (Å)	Exo		Endo		Both
	Expt ^a	Calc ^b	Expt ^a	Calc ^b	Expt ^a
Cr—S	2.344(1)	2.372	2.356(1)	2.388	2.351(1)
S—S	2.121(1)	2.211	2.142(1)	2.202	2.134(2)
S—N	1.638(3)	1.648	1.638(4)	1.654	1.638(4)
N—C	1.336(4)	1.330	1.334(6)	1.329	1.335(5)

526 ^a Average over all indicated crystallographic values; errors are root mean squares.

527 ^b From B3PW91/6-311+G(2d,2p)// B3PW91/6-31G(d) calculations within C_{2v} symmetry

528

529 These calculations also provide insights into the formal resemblance between the bonding
 530 of dithiadiazolylys with CpCr(CO)₂ and π-allyl complexes (note that the directly analogous π-
 531 allyls to **3**, CpCr(CO)₂[R₂CC(R)CR₂], have only recently been characterized).⁶⁵



Scheme 4

532

533

534

535 Consideration of the frontier π -orbitals of (a) the allyl radical and (b) the highest three of
 536 HCN_2S_2 (Scheme 4) emphasizes the similarity between the two systems. Topologically, π_4 of the
 537 dithiadiazolyl resembles allyl π_2 , while π_3 of the heterocycle resembles allyl π_1 . The separation
 538 between the terminal C atoms of the allyl at ~ 2.4 Å is only a little larger than the ~ 2.1 Å between
 539 the two sulfur atoms of the dithiadiazolyl, and the p orbitals of the latter are expected to have
 540 larger effective radii, further minimizing the effect of any differences in ligand size.
 541 Energetically, these two pairs of orbitals are also similar while the lower π orbitals of the
 542 heterocycle are of no consequence in metal binding due to the high effective electronegativity of
 543 both nitrogen and sulphur.⁶¹ The fact that the π -allyl complexes with $\text{CpCr}(\text{CO})_2$ are also known
 544 to form both *exo* and *endo* isomers – albeit non-inter-converting – strengthens the bonding
 545 analogy.⁶⁵

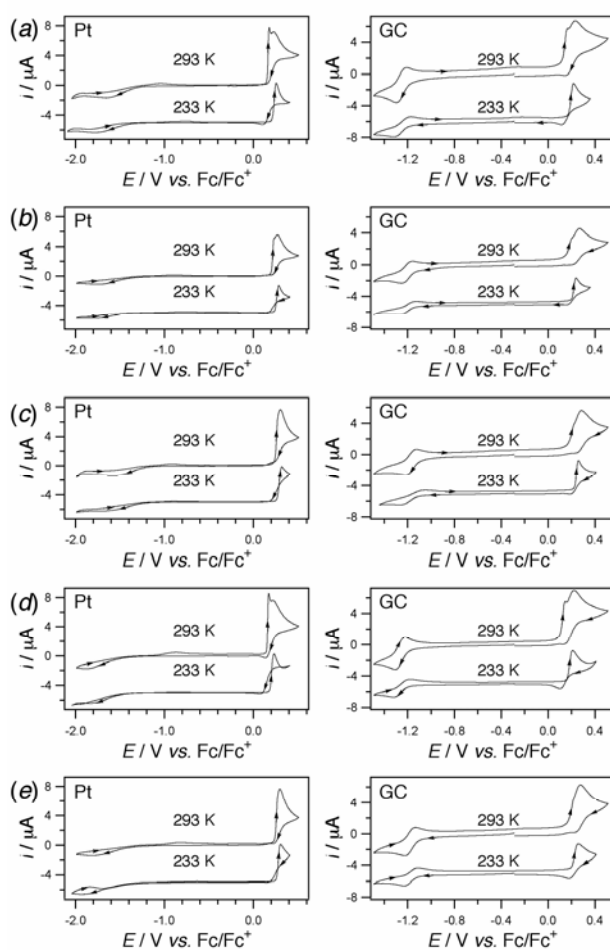
546

547 3.7 Electrochemistry

548 The cyclic voltammograms obtained of CH_3CN solutions containing **3a-e** at two different
 549 temperatures at Pt and GC electrodes are displayed in Figure 5, with all compounds giving rise to
 550 an oxidation and reduction process. On Pt, the reduction process appeared very drawn out, with
 551 an extremely wide separation between the forward and reverse peaks (~ 1 V). On GC, the
 552 reduction process appeared chemically reversible, although the anodic (E_p^{ox}) to cathodic (E_p^{red})
 553 peak-to-peak separations ΔE_{pp} were slightly wider than expected for a one-electron process
 554 (Table 4). Therefore, it is likely that the reduction process is affected by a slow rate of
 555 heterogeneous electron transfer, which is particularly slow on Pt.

556 The oxidation processes were complicated on both Pt and GC electrodes (Figure 5). On
 557 Pt, the E_p^{ox} peaks were particularly steep and the reverse current-potential traces often
 558 overlapped with the forward current-potential traces, especially at low temperature. Such
 559 behavior is typical of compounds that undergo adsorption during the electron transfer process.

560 On GC, the same voltammetric features (steep E_p^{ox} peak and overlapping current-potential traces)
 561 were evident but to a lesser extent than on Pt, suggesting less adsorption. The anodic peak
 562 current (i_p^{ox}) for the oxidative process was much greater than the cathodic peak current (i_p^{red}) for
 563 the reduction process, suggesting more electrons were transferred during the oxidation, although
 564 peak currents are not necessarily indicative of the relative number of electrons transferred in
 565 processes that involve adsorption. It is likely that the reduction processes (on GC) involves the
 566 chemically reversible transfer of one-electron while the oxidative processes involves the transfer
 567 of greater than one-electron. The chemical reversibility of the oxidation processes appeared to
 568 improve on GC as the temperature was lowered, especially for compounds **3a**, **3d** and **3e**, in the
 569 sense that the $i_p^{\text{red}}/i_p^{\text{ox}}$ ratio became closer to unity at lower temperatures.



570
 571
 572 **Figure 5.** Cyclic voltammograms recorded at 100 mV s^{-1} at 1 mm planar Pt or GC electrodes in
 573 CH_3CN with $0.25 \text{ M } n\text{Bu}_4\text{NPF}_6$ of 1 mM solutions of (a) **3a**, (b) **3b**, (c) **3c**, (d) **3d**, and (e) **3e**.
 574 Voltammograms at 233 K are offset by $-5 \mu\text{A}$.

575

576 3.8 SEEPR

577 Depending on sample history, solutions of **3a-e** in CH₃CN/0.1 M ⁿBuNPF₆ displayed either a flat
578 baseline or small EPR signals (a five-line with $a_N = 0.51$ mT, $g = 2.010$ and a single-line, $g =$
579 1.981 , $LW = 0.3$ mT, $a_{Cr} = 0.85$ mT) consistent with minor dissociation into free **2A**⁵⁹ and a Cr-
580 centred radical, though the g value of the latter is quite different from that expected for
581 CpCr(CO)₂NCCH₃, the solvate which might reasonably result from a simple dissociation of the
582 complex into two free radicals. (For example, g for CpCr(CO)₂NCPh is reported to be 2.025;⁶⁶
583 the g we observe is more typical of a Cr⁺³ species.)⁶⁷ Upon electrolysis at the peak potentials
584 corresponding to the oxidation processes, no new EPR signals were obtained. This is consistent
585 with the CV evidence for >1 electron transfer, leading either to diamagnetic products *via*
586 chemical steps following the heterogeneous electron transfers, or to instant adsorption onto the
587 electrode surface. However, upon electrolysis at the cathodic peak potentials for the reduction
588 processes listed in Table 4, a strong new five-line pattern rapidly evolves (Figure 6) which
589 overwhelms any minor impurity signals present. The spectra of all five radicals are very similar
590 with narrow spectral lines and hfc constants of 0.587 – 0.597 mT to two equivalent $I = 1$ nuclei,
591 i.e. two ¹⁴N (Table 4). There is no evidence for hfc to ⁵³Cr ($I = 3/2$, 9.5% abund), as satellites of
592 4.75% intensity even with small a_{Cr} values should easily be observable about the sharp main
593 spectral lines. Against the notion that the EPR spectra belong to free **2A** are the ~0.1 mT larger
594 hfc (*all* these dithiadiazolyl radicals have hfc of 0.51 mT to two equivalent ¹⁴N nuclei)^{59,34b} and
595 the short half-lives (4 – 6 s, see Table 4), whereas dithiadiazolyls are stable radicals in absence of
596 O₂. These spectra are thus fully consistent with *ligand-centred* reduction of complexes **3a-e**
597 resulting in complexed radical anions **3a-e**⁻ that are stabilized by CH₃CN solvent, but which
598 decay either by dissociation into **1A** and **2A**⁻ or **1A**⁻ and **2A**, or else by adsorption to the cell
599 walls or onto the gold electrodes. Consistent with this, samples which had undergone repeated
600 electrolyses showed after the decay of the signals from **3**⁻ significantly more intense, persistent,
601 signals ($g = 2.010$) attributable to **2A** as well as overlapping signals of varying LW at $g = 2.002 -$
602 2.003 with the appearance of axial powder patterns with small g anisotropies (~0.006). We
603 attribute these latter species to radicals adsorbed on surfaces, whether organic or Cr-containing
604 cannot be ascertained.

605

606 **Table 4. Cyclic voltammetric ^a and EPR data.**

607

Compound	Reduction Processes				EPR Data from One-Electron Reduced Compounds (Anion Radicals) $3^{\bullet-}$			
	$E_p^{\text{red}} / \text{V}^b$	$E_p^{\text{ox}} / \text{V}^c$	$E_{1/2}^r / \text{V}^d$	$\Delta E / \text{mV}^e$	g^f	a_N / mT^g	LW/mT ^h	$t_{1/2} / \text{s}$
3a	-1.296	-1.212	-1.25	84	2.0085	0.597	0.072	5.7
3b	-1.252	-1.160	-1.21	92	2.0086	0.591	0.071	4.1
3c	-1.218	-1.124	-1.17	94	2.0085	0.597 ⁱ	0.069	5.6
3d	-1.226	-1.134	-1.18	92	2.0088	0.589 ^j	0.073	5.7
3e	-1.306	-1.222	-1.26	84	2.0088	0.587	0.072	4.0

608

609 ^a Obtained at a scan rate of 100 mV s⁻¹ at a 1 mm diameter GC electrode at 293 K in CH₃CN with
610 0.25 M Bu₄NPF₆ as the supporting electrolyte; all potentials are relative to the
611 ferrocene/ferrocenium redox couple.

612 ^b E_p^{red} = reductive peak potential.

613 ^c E_p^{ox} = oxidative peak potential.

614 ^d $E_{1/2}^r = (E_p^{\text{red}} + E_p^{\text{ox}}) / 2$ (measured to nearest 10 mV).

615 ^e $\Delta E = |E_p^{\text{ox}} - E_p^{\text{red}}|$.

616 ^f Measured against solid DPPH; 2.0037 ± 0.0002

617 ^g At 291 K in CH₃CN containing 0.1 M Bu₄NPF₆ unless otherwise noted; a_N values were found
618 to be independent of temperature over the range 233 – 291 K for all $3^{\bullet-}$.

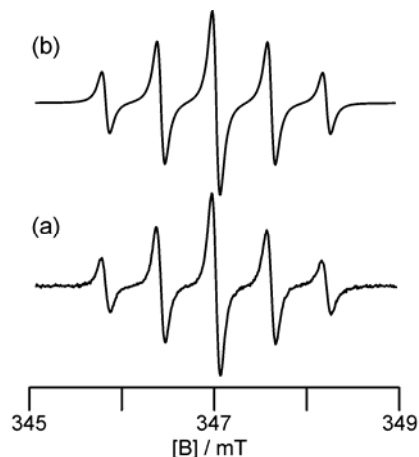
619 ^h Peak-to-peak linewidth in dispersion mode obtained from digital simulation in WinSim 2002, ⁴⁵
620 and independent of T over the range 233 – 291 K for all $3^{\bullet-}$.

621 ⁱ At 253 K in CH₃CN containing 0.1 M Bu₄NPF₆.

622 ^j At 270 K in CH₃CN containing 0.1 M Bu₄NPF₆.

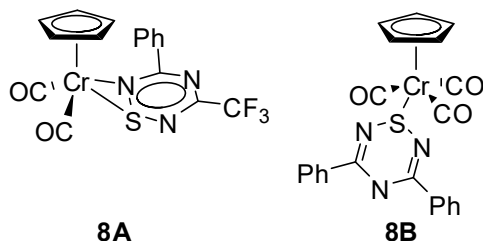
623

624



625
626
627 **Figure 6.** Experimental (a) and simulated (b) (WinSim 2002) EPR spectrum obtained upon the
628 *in situ* electrolysis at 291 K of (8.1 mM) **3a** in CH₃CN / ⁿBu₄PF₆ (0.1 M) solution at a potential
629 of -1.30 V vs. Fc. The simulation employed Lorentzian lineshapes with a LW of 0.072 mT, $a_N =$
630 0.597 mT and $g = 2.0085$ measured against solid external dpph.

631
632 The a_N values of **3a-e⁻** are independent of temperature over the range 233 K to 291 K. A
633 subtle trend in the size of the hfc can be observed from 0.587 for the most electron-withdrawing
634 aryl substituent to 0.597 mT for the donating OMe group. Curiously, no such trend is seen in the
635 $E_{1/2}$ values. These a_N values suggest that spin density within the S₂N₂C ring is polarized towards
636 the nitrogen atoms (and away from sulfur) compared to **2A**. The spectral lines are much narrower
637 than those of dithiadiazolyls at 291 K, and do not show the temperature dependence of the LW
638 displayed by the latter.^{34b} The line shapes are fully Lorentzian, indicating the absence of
639 unresolved hfc e.g. to aryl ring ¹H nuclei. However, the absence of ⁵³Cr hfc augurs against a
640 structure for the anions directly analogous to that of the neutral complexes **3** (based on results
641 from DFT calculations on the anion at the neutral-complex geometry). A possible insight into
642 this conundrum is provided by our recent discovery of two distinct side-on π bonding modes for
643 the complexes between **1A** and two 7π 1,2,4,6-thiatriazinyls (hence closely related to **2**): η^2
644 (three-electron donating) in **8A** and η^1 (one-electron donating) in **8B**.⁵⁶



645

646 It is therefore possible that, upon reduction, the dithiadiazolyl ligands are partly displaced to a
647 more weakly-bonded η^1 coordination mode, with CH₃CN taking the 5th ligand position occupied
648 by the third CO in **8B**. We are inclined to this view, despite the apparently symmetric spectra
649 (equivalent ¹⁴N nuclei). The bonding may be fluxional between the two S atoms in the solution
650 phase, or a minor asymmetry in hfc may be too small to resolve given the rather large spectral
651 linewidths. What we have not yet established is whether this specific solvation by CH₃CN
652 precedes, or follows, the one-electron reduction process.

653 **4. Conclusions**

654 The interaction between [CpCr(CO)₃]₂ and dithiadiazolyl dimers [S₂N₂CNR]₂ (R = substituted
655 aryl rings) has resulted in the isolation of a series of the first π organometallic complexes of
656 C,N,S-heterocyclic compounds. X-ray diffraction analyses revealed that these heterocyclic
657 ligands are η^2 -S,S'-bonded to the Cr center and are oriented either *endo* or *exo* with respect to the
658 Cp ring. Thorough chemical studies demonstrate that formation of **3a-e** competes with their
659 destruction by as yet unreacted **1**, leading to complex reaction mixtures. A dynamic NMR study
660 of the complex with R = 4-CF₃C₆H₄ identified a likely intramolecular exchange process with an
661 appreciable ΔG_{298}^\ddagger of 59±4 kJ mol⁻¹ as well as a minor dissociative process that remains in fast
662 exchange over the temperature range 200 – 300 K. The measured enthalpies and equilibrium
663 populations are in accord with data from gas-phase DFT calculations which indicate that the two
664 isomers are very similar in energy, with the *endo* being 3±1 kJ mol⁻¹ more stable. Cyclic
665 voltammetry experiments indicated that **3a-e** could be reduced in a one-electron process and
666 oxidized in a multi-electron process. However, the appearance of the oxidation/reduction
667 processes is strongly influenced by the electrode surface (Pt or GC). On Pt, the reduction
668 processes were affected by slow rates of heterogeneous electron transfer while the oxidation
669 processes showed evidence of adsorption. *In situ* electrochemical-EPR spectroscopy experiments
670 performed during the one-electron reduction of **3a-e** led to the detection of semi-stable anion
671 radicals, whose half-lives were estimated by measuring the decrease in EPR signal intensities
672 over time (average $t_{1/2} \sim 6$ s at 291 K). These results speak to a versatile and largely unexplored
673 coordination chemistry of unsaturated C-N-S heterocyclic free radicals with paramagnetic
674 organometallic species. Further investigations of this kind are underway in our laboratories.

675 **Supporting Information Available**

676 X-ray crystallographic files in CIF format of **3a – e** and **2d**. *Figure S1*. Temperature
677 dependence of the ¹H NMR spectra of **3d** between 200 and 300 K. *Figure S2*. Detailed

678 DNMR linefits at all measured temperature for **3d** for the aromatic region. *Figure S3*.
679 DNMR linefits for the Cp region. *Figure S4*. Plots of $\ln K$ vs. $1/T$. *Figure S5*. Eyring
680 plots for the exchange rate study of **3d** from the Cp spectral region. *Figure S6*. Atom-
681 labels, and full geometric details for the optimized *exo* and *endo* isomers, from DFT
682 calculations. *Figure S7*. Enlarged CV's from Figure 5. *Figure S8*. Diagrams showing
683 the four dimers of **2d** and the unit cell packing. *Table S1*. Equilibrium Constants from
684 the DNMR Study of **3d**. *Table S2*. Rate data from the DNMR study on **3d**. *Table S3*.
685 Summary of DNMR results. This material is available free of charge via the Internet at
686 <http://pubs.acs.org>.

687

688 **Acknowledgements**

689 Support from the Natural Sciences and Engineering Research Council and the Alberta Ingenuity
690 Fund of Canada, the National University of Singapore for Academic Research Grant no. R143-
691 000-209-112 (LYG) and postgraduate scholarships (VWLN, SLK and TLR) and the Nanyang
692 Technological University (RDW and LYG), is gratefully acknowledged. The authors also thank
693 L. L. Koh and G. K. Tan for X-ray diffraction analyses and R. P. A. Bettens and Y. Fan for
694 preliminary calculations performed using B3LYP/LANL2DZ.

695

696 **References and Notes**

- 697 (1) Goh, L. Y. *Coord. Chem. Rev.* **1999**, *185-186*, 257-276 and references therein.
- 698 (2) (a) Goh, L. Y.; Tay, M. S.; Mak, T. C. W.; Wang, R.-J. *Organometallics* **1992**, *11*, 1711-
699 1717. (b) Goh, L. Y.; Tay, M. S.; Lim, Y. Y.; Mak, T. C. W.; Zhou, Z.-Y. *J. Chem. Soc.,*
700 *Dalton Trans.* **1992**, 1239-1242. (c) Goh, L. Y.; Tay, M. S.; Chen, W. *Organometallics*
701 **1994**, *13*, 1813-1820.
- 702 (3) Goh, L. Y., Leong, W. K., Leung, P.-H., Weng, Z., Haiduc, I. *J. Organomet. Chem.* **2000**,
703 *607*, 64-71.
- 704 (4) Goh, L. Y.; Weng, Z.; Leong, W. K.; Haiduc, I.; Lo, K. M.; Wong, R. C. S. *J. Organomet.*
705 *Chem.* **2001**, *631*, 67-75.
- 706 (5) (a) Goh, L. Y.; Weng, Z.; Leong, W. K.; Leung, P. H. *Angew. Chem. Int. Ed.* **2001**, *40*,
707 3236-3239. (b) Goh, L. Y.; Weng, Z.; Leong, W. K.; Leung, P. H. *Organometallics* **2002**,
708 *21*, 4398-4407. (c) Goh, L. Y.; Weng, Z.; Hor, T. S. A.; Leong, W. K. *Organometallics*
709 **2002**, *21*, 4408-4414.

- 710 (6) Goh, L. Y.; Weng, Z.; Leong, W. K.; Vittal, J. J. *J. Am. Chem. Soc.* **2002**, *124*, 8804-
711 8805.
- 712 (7) Ng, V. W. L.; Weng, Z.; Vittal, J. J.; Koh, L. L.; Tan, G. K.; Goh, L. Y. *J. Organomet.*
713 *Chem.* **2005**, *690*, 1157-1165.
- 714 (8) (a) Goh, L. Y.; Chen, W.; Wong, R. C. S. *Angew Chem., Int. Ed. Engl.* **1993**, *32*, 1728-
715 1729. (b) Goh, L. Y.; Chen, W.; Wong, R. C. S.; Karaghiosoff, K. *Organometallics* **1995**,
716 *14*, 3886-3896.
- 717 (9) Goh, L. Y.; Chen, W.; Wong, R. C. S. *Organometallics* **1999**, *18*, 306-314.
- 718 (10) Goh, L. Y.; Chen, W.; Wong, R. C. S. *Chem. Commun.* **1999**, 1481-1482.
- 719 (11) (a) Weng, Z.; Leong, W. K.; Vittal, J. J.; Goh, L. Y. *Organometallics* **2003**, *22*, 1645-
720 1656. (b) Weng, Z.; Leong, W. K.; Vittal, J. J.; Goh, L. Y. *Organometallics* **2003**, *22*,
721 1657-1662.
- 722 (12) Weng, Z.; Goh, L. Y. *Acc. Chem. Res.* **2004**, *37*, 187-199 and references therein.
- 723 (13) (a) Brooks, W. V. F.; Burford, N.; Passmore, J.; Schriver, M. J.; Sutcliffe, L. H. *J. Chem.*
724 *Soc., Chem. Commun.* **1987**, 69-71. (b) Fairhurst, S. A.; Johnson, K. M.; Sutcliffe, L. H.;
725 Preston, K. F.; Banister, A. J.; Hauptman, Z. V.; Passmore, J. *J. Chem. Soc., Dalton*
726 *Trans.* **1986**, 1465-1472.
- 727 (14) (a) Aherne, C.; Banister, A. J.; Luke, A. W.; Rawson, J. M.; Whitehead, R. J. *J. Chem.*
728 *Soc., Dalton Trans.* **1992**, 1277-1282. (b) Banister, A. J.; Lavender, I.; Rawson, J. M.;
729 Clegg, W.; Tanner, B. K.; Whitehead, R. J. *J. Chem. Soc., Dalton Trans.* **1993**, 1421-
730 1429. (c) Banister, A. J.; Batsanov, A. S.; Dawe, O. G.; Herbertson, P. L.; Howard, J. A.
731 K.; Lynn, S.; May, I.; Smith, J. N. B.; Rawson, J. M.; Rogers, T. E.; Tanner, B. K.;
732 Antorrena, G.; Palacio, F. *J. Chem. Soc., Dalton Trans.* **1997**, 2539-2542.
- 733 (15) See the following articles/reviews and references therein: (a) Banister, A. J.; Rawson, J.
734 M. *Chemistry in Britain* **1992**, 148-152. (b) Cordes, A. W.; Haddon, R. C.; Oakley, R. T.
735 in Steudel, R. (Ed.), *Studies in Inorganic Chemistry, Vol. 14: The Chemistry of Inorganic*
736 *Ring Systems*, Elsevier, Amsterdam **1992**, *Ch. 16*, p. 295-348. (c) Rawson, J. M.; Banister,
737 A. J.; Lavender, I. *Adv. Heterocycl. Chem.* **1995**, *62*, 137-247. (d) Rawson, J. M.; Palacio,
738 F. *Structure and Bonding* **2001**, *100*, 93-128. (e) Alberola, A.; Less, R. J.; Pask, C. M.;
739 Rawson, J. M.; Palacio, F.; Oliete, P.; Paulsen, C.; Yamaguchi, A.; Farley, R.D.; Murphy,
740 D. M. *Angew. Chem. Int. Ed.* **2003**, *42*, 4782-4785. (f) Boéré, R. T.; Moock, K. H.

- 741 *Phosphorus, Sulfur, and Silicon* **1994**, 93-94, 451-452. (g) Rawson, J. M.; Alberola, A.;
742 Whalley, A. *J. Mat. Chem.* **2006**, 16, 2560-2575.
- 743 (16) Cordes, A. W.; Haddon, R. C.; Oakley, R. T. *Adv. Mater.* **1994**, 6, 798-802.
- 744 (17) (a) Boéré, R. T.; Moock, K. H.; Klassen, V.; Weaver, J.; Lentz, D.; Michael-Schulz, H.
745 *Can. J. Chem.* **1995**, 73, 1444-1453. (b) Klassen, V.; Preuss, K.; Moock, K. H.; Boéré, R.
746 T. *Phos., Sulf. Silicon*. **1994**, 93-94, 449-450.
- 747 (18) Banister, A. J.; Gorrell, I. B.; Clegg, W.; Jørgensen, K. A. *J. Chem. Soc. Dalton Trans.*
748 **1989**, 2229-2233.
- 749 (19) Banister, A. J.; Gorrell, I. B.; Clegg, W.; Jørgensen, K. A. *J. Chem. Soc. Dalton Trans.*
750 **1991**, 1105-1109.
- 751 (20) Banister, A. J.; Gorrell, I. B.; Lawrence, S. E.; Lehmann, C. W.; May, I.; Tate, G.; Blake,
752 A. J.; Rawson, J. M. *J. Chem. Soc. Chem. Commun.* **1994**, 1779-1780.
- 753 (21) Banister, A. J.; May, I. *Phos., Sulf. Silicon* **1994**, 93-94, 447-448.
- 754 (22) Banister, A. J.; Howard, J. A. K.; May, I.; Rawson, J. M. *J. Chem. Soc. Chem. Commun.*
755 **1997**, 1763-1764.
- 756 (23) Banister, A. J., Gorrell, I. B.; Howard, J. A. K.; Lawrence, S. E.; Lehman, C. W.; May, I.;
757 Rawson, J. M.; Tanner, B. K.; Gregory, C. I.; Blake, A. J.; Fricker, S. P. *J. Chem. Soc.*
758 *Dalton Trans.* **1997**, 377-384.
- 759 (24) Banister, A. J.; May, I.; Rawson, J. M.; Smith, J. N. B. *J. Organomet. Chem.* **1998**, 550,
760 241-253 (review) and references therein.
- 761 (25) Wong, W-K.; Sun, C.; Wong, W-Y.; Kwong, D. W. J.; Wong, W. T. *Eur. J. Inorg. Chem.*
762 **2000**, 1045-1054.
- 763 (26) Preuss, K. E. *Dalton Trans.* **2007**, 2357-2369.
- 764 (27) See for instance the following: (a) Adams, R. D.; Collins, D. E.; Cotton, F. A. *J. Am.*
765 *Chem. Soc.* **1974**, 96, 749-754. (b) Madach, T.; Vahrenkamp, H. *Z. Naturforsch. B.* **1978**,
766 33b, 1301-1303. (c) Goh, L. Y.; D'Aniello, M. J., Jr.; Slater, S.; Muetterties, E. L.;
767 Tavanaiepour, I.; Chang, M. I.; Fredrich, M. F.; Daz, V. W. *Inorg. Chem.* **1979**, 18, 192-
768 197. (d) McLain, S. J. *J. Am. Chem. Soc.* **1988**, 110, 643-644. (e) Baird, M. C. *Chem. Rev.*
769 **1988**, 88, 1217-1227. (f) Goh, L. Y.; Lim, Y. Y. *J. Organomet. Chem.* **1991**, 402, 209-
770 214.
- 771 (28) (a) Lau, H. F.; Ng, V. W. L.; Koh, L. L.; Tan, G. K.; Goh, L. Y.; Roemmele, T. L.;
772 Seagrave, S. D.; Boéré, R. T. *Angew Chem., Int. Ed. Engl.*, **2006**, 45, 4498-4501. (b)

- 773 Boéré, R. T.; Roemmele, T. L.; Seagrave, S. D.; Goh, L. Y. 88th Canadian Chemistry
774 Conference and Exhibition, Saskatoon, Canada. May 28-June 1, 2005, Abstract #490. (c)
775 Boéré, R. T.; Yu., X.; Goh, L.-Y.; Ng, V. W. L.; Ang, C. W. P.; Kuan S. L.; Lau, H. F.
776 89th Canadian Chemistry Conference and Exhibition, Halifax, NS, Canada, May 27 – 31,
777 2006 (Abstract #0061).
- 778 (29) (a) Hearn, N. G. R.; Preuss, K. E.; Richardson, J. F.; Bin-Salamon, S. *J. Am. Chem. Soc.*
779 **2004**, *126*, 9942-9943. (b) Britten, J.; Hearn, N. G. R.; Preuss, K. E.; Richardson, J. F.;
780 Bin-Salamon, S. *Inorg. Chem.* **2007**, *46*, 3934-3945.
- 781 (30) (a) Jennings, M.; Preuss, K. E.; Wu, J. *Chem. Commun.* **2006**, 341. (b) Hearn, N. G. R.;
782 Hesp, K. D.; Jennings, M.; Korčok, J. L.; Preuss, K. E.; Smithson, C. S. *Polyhedron*
783 **2007**, *26*, 2047-2053.
- 784 (31) Bénard, M. *Nouv. J. Chim.* **1986**, *10*, 529-532.
- 785 (32) (a) Van Droogenbroeck, J.; Van Alsenoy, C.; Aucott, S. M.; Woollins, J. D.; Hunter, A.
786 D.; Blockhuys, F. *Organometallics* **2005**, *24*, 1004-1011. (b) Aucott, S. M.;
787 Bhattacharyya, P.; Milton, H. L.; Slawin, A. M. Z.; Woollins, J. D. *New J. Chem.* **2003**,
788 *27*, 1466-1469. (c) Aucott, S. M.; Slawin, A. M. Z.; Woollins, J. D. *Can. J. Chem.* **2002**,
789 *80*, 1481-1487. (d) Boéré, R. T.; Klassen, B.; Mook, K. H. *J. Organomet. Chem.* **1994**,
790 *467*, 127-133. (e) Chivers, T.; Edlmann, F. *Polyhedron* **1986**, *5*, 1661-1669. (f) Kelly, P.
791 F.; Woollins, J. D. *Polyhedron* **1986**, 607-632.
- 792 (33) Manning, A. R.; Hackett, P.; Birdwhistell, R.; Soye, P. *Inorg. Synth.* **1990**, *28*, 148-150.
- 793 (34) (a) Boéré, R. T.; Mook, K. H.; Derrick, S.; Hoogerdijk, W.; Preuss, K.; Yip, J.; Parvez,
794 M. *Can. J. Chem.* **1993**, *71*, 473-486. (b) Boéré, R. T.; Goh, L. Y.; Ang, C. Y.; Kuan, S.
795 L.; Lau, H. F.; Ng, V. W. L.; Roemmele, T. L.; Seagrave, S. D. *J. Organomet. Chem.*
796 **2007**, *692*, 2697-2704.
- 797 (35) Chen, W.; Goh, L. Y.; Mak, T. C. W. *Organometallics* **1986**, *5*, 1997-2002.
- 798 (36) Ernest, I.; Holick, W.; Rihs, G.; Schomburg, D.; Shoham, G.; Wenkert, D.; Woodward, R.
799 B. *J. Am. Chem. Soc.* **1981**, *103*, 1540-1544.
- 800 (37) Behrens, U.; Edlmann, F. *J. Organomet. Chem.* **1984**, *263*, 179-182.
- 801 (38) (a) Greenhough, T. J.; Kolthammer, B. W. S.; Legzdins, P.; Trotter, J. *Inorg. Chem.* **1979**,
802 *18*, 3543-3548. (b) Goh, L. Y.; Hambley, T. W.; Robertson, G. B. *J. Chem. Soc., Chem.*
803 *Commun.* **1983**, 1458-1460. (c) Goh, L. Y.; Hambley, T. W.; Robertson, G. B.
804 *Organometallics* **1987**, *6*, 1051-1057.

- 805 (39) R. A. Beekman, R. T. Boéré, K. H. Moock, M. Parvez, *Can. J. Chem.*, **1998**, *76*, 85-93.
- 806 (40) SMART & SAINT Software Reference manuals, version 5.0, Bruker AXS Inc.,Madison,
807 WI, 1998.
- 808 (41) Sheldrick, G. M. SADABS software for empirical absorption correction; University of
809 Göttingen: Germany, 2000.
- 810 (42) SHELXTL Reference Manual, version 5.1, Bruker AXS Inc., Madison, WI, 1998.
- 811 (43) (a) Boéré, R. T.; Bond, A. M.; Chivers, T.; Feldberg, S. W.; Roemmele, T. L. *Inorg.*
812 *Chem.* **2007**, *46*, 5596-5607. (b) Neudeck, A.; Kress, L. *J. Electroanal. Chem.* **1997**, *437*,
813 141-156.
- 814 (44) Boéré R. T.; Roemmele, T. L. *In preparation*.
- 815 (45) WinSim (v.0.98, 2002) software: Duling, D. R. *J. Mag. Res. B.* **1994**, *104*, 105-110.
- 816 (46) Gaussian 98W, Revision A.9, M. J. Frisch, *et al.* Gaussian, Inc., Pittsburg, PA, 1998.
- 817 (47) Becke, A. D. *J. Chem. Phys.* **1993**, *98*, 5648-5652.
- 818 (48) Perdew, J. P.; Wang, Y. *Phys. Rev. B.* **1992**, *45*, 13244-13249.
- 819 (49) Carlson, C. N.; Smith, J. D.; Hanusa, T. P.; Brennessel, W. W.; Young, V. G., Jr. *J.*
820 *Organomet. Chem.* **2003**, *683*, 191-199.
- 821 (50) McConnel, H. M. *J. Chem. Phys.* **1956**, *28*, 430-431.
- 822 (51) Mathworks, Inc., Matlab 6.5 (2002).
- 823 (52) Fano, U. *Rev. Mod. Phys.* **1957**, *29*, 74-93.
- 824 (53) (a) Bain, A. D.; Cramer, J. A. *J. Phys. Chem.* **1993**, *97*, 2884-2887. (b) Bain, A. D.;
825 Cramer, J. A. *J. Magnet. Reson. A.* **1993**, *103*, 217-222.
- 826 (54) Bain, A. D.; Duns, G. J.; Ternieden, S.; Ma, J.; Werstiuk, N. H. *J. Phys. Chem.* **1994**, *98*,
827 7458-7463.
- 828 (55) For data sets obtained over large temperature ranges, errors in the enthalpy can be as
829 small as 1 kJ/mol and in the entropy as small as 5 J/mol K: Bain, A. D.; Hazendonk, P. *J.*
830 *Phys. Chem. A.* **1997**, *101*, 7182-7188.
- 831 (56) We use the term *redox compatible* to mean species with overlapping redox stability
832 windows, for which the driving force for an immediate electron transfer reaction is absent:
833 Ang, C. W.; Boéré, R. T.; Goh, L. Y.; Koh, L. L.; Kuan, S. L.; Tan, G. K.; Yu, X. *Chem.*
834 *Commun.* **2006**, 4735-4737.
- 835 (57) Boéré, R. T.; Roemmele, T. L. *Coord. Chem. Rev.* **2000**, *210*, 369-445.

- 836 (58) Barbini, D. C.; Tanner, P. S.; Francone, T. D.; Furst, K. B.; Jones, W. E. *Inorg. Chem.*
837 **1996**, *35*, 4017-4022.
- 838 (59) Boéré, R. T.; Mook, K. H.; Parvez, M. Z. *Anorg. Allg. Chem.* **1994**, *620*, 1589-1598.
- 839 (60) The unit cell of **2d** contains eight monomeric F₃CC₆H₄CN₂S₂ rings in the asymmetric
840 unit (Figure S8), each arranged to give four distinct *cis*-cofacial dimers, each of which
841 has a different manifestation of steric distortion to accommodate the bulky CF₃ group.
842 These dimers associate in two zones within the lattice: in the first, four dimers aggregate
843 around an approximate four-fold axis in a “pin-wheel” motif that has been observed
844 previously for DTDA structures. In the second, six dimer pairs align side-by side in sets
845 of three. In each case, there are short cross-ring S⋯N interactions. In addition, there are
846 considerably longer S⋯S and S⋯N contacts in the stacking direction. Such complexity
847 has been seen previously in DTDA crystal structures, with 2 of the 45 reported neutral
848 DTDA structures contained in the CSD (V 5.28, 2007) having the same number of
849 monomers per equivalent position. Specifically, a long-known structure of CH₃CN₂S₂
850 crystallizes in the same space group as **2d**: Banister, A. J., Hansford, M. I., Hauptman, Z.
851 V., Wait, S. T., Clegg, W. *J. Chem. Soc., Dalton Trans.* **1989**, 1705-1713. A more
852 recently reported polymorph of ClCN₂S₂ – which like **2d** was collected at low temperature
853 – crystallizes in *P2₁/c*: Bond, A. D.; Haynes, D. A.; Pask, C. M.; Rawson, J. M. *J. Chem.*
854 *Soc., Dalton Trans.* **2002**, 2522-2531. The closely related compound 4-CF₃-3-F-
855 C₆H₃CN₂S₂ shows similar steric distortions as found in **2c**, though it crystallizes with
856 only 4 monomers per equivalent position in $\bar{P}1$: Clarke, C. S.; Haynes, D. A.; Rawson, J.
857 M.; Bond, A. D. *Chem. Commun.* **2003**, 2774-2775. As commonly observed in such
858 structures, the dominant local pairing into dimers – a manifestation of the Peierls
859 distortion – prevents the long-range contacts essential for a conducting state.
- 860 (61) Oakley, R. T. *Prog. Inorg. Chem.* **1988**, *36*, 299-391.
- 861 (62) Ng, V. W. L.; Kuan, S. L.; Weng, Z.; Leong, W. K.; Vittal, J. J.; Koh, L. L.; Tan, G. K.;
862 Goh, L. Y. *J. Organomet. Chem.* **2005**, *690*, 2323-2332.
- 863 (63) Nyburg, S. C.; Faerman, C. H. *Acta Crystallogr., Sect. B.* **1985**, *41*, 274-279.
- 864 (64) The existence of the 8π anion has only been demonstrated electrochemically on the time-
865 scale of cyclic voltammetry, see ref. (57).
- 866 (65) Norman, D. W.; Ferguson, M. J.; Stryker, J. M. *Organometallics* **2004**, *23*, 2015-2019.

- 867 (66) Morton, J. R.; Preston, K. F.; Cooley, N. A.; Baird, M. C.; Krusic, P. J.; McLain, S. J. *J.*
868 *Chem. Soc., Faraday Trans.* **1987**, *83*, 3535-3540.
- 869 (67) (a) Atsarkin, V. A.; Gerasimova, É. A.; Matveeva, I. G.; Frantsesson, A. V. *Sov. Phys.*
870 *JEPT* **1963**, *16*, 903. (b) Henderson, B.; Wertz, J. E. *Defects in the Alkaline Earth Oxides*,
871 Halstead-Wiley, New York, NY, **1977**, p. 37.

872 **Graphical Abstract**

873

874 **Coupling of CpCr(CO)₃ and Heterocyclic Dithiadiazolyl Radicals. Synthetic, X-ray**
875 **diffraction, dynamic NMR, EPR, CV and DFT studies.**

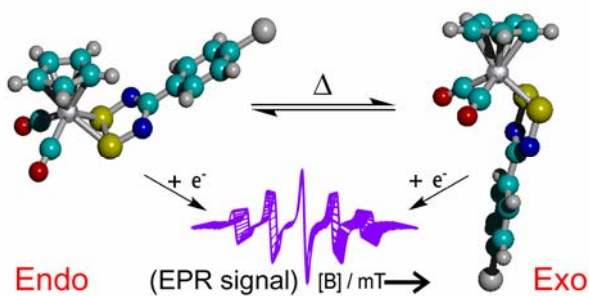
876

877 **Hiu Fung Lau, Pearly Chwee Ying Ang, Victor Wee Lin Ng, Seah Ling Kuan, Lai Yoong**
878 **Goh, Alexey S. Borisov, Paul Hazendonk, Tracey L. Roemmele, René T. Boéré, and**
879 **Richard D. Webster**

880

881

882 Unique diamagnetic π -complexes of 1,2,3,5-dithiadiazolyls with CpCr(CO)₂ fragments are η^2 -
883 S,S'-coordinated to the metal in *endo* and *exo* fashion, inter-convert between isomers in solution
884 and remain redox-active through ligand-centered reductions.



Coupling of CpCr(CO)₃ and Heterocyclic Dithiadiazolyl Radicals. Synthetic, X-ray diffraction, dynamic NMR, EPR, CV and DFT studies.

Hui Fung Lau,^(a) Pearly Chwee Ying Ang,^(a) Victor Wee Lin Ng,^(a) Seah Ling Kuan,^(a) Lai Yoong Goh,^{(a)*†} Alexey S. Borisov,^(b) Paul Hazendonk,^(b) Tracey L. Roemmele,^(b) René T. Boéré,^{(b)*‡} and Richard D. Webster^(c)

^(a) Department of Chemistry, National University of Singapore, Kent Ridge, Singapore 119260

^(b) Department of Chemistry and Biochemistry, University of Lethbridge, Lethbridge, Alberta, Canada T1K 3M4

^(c) Division of Chemistry and Biological Chemistry, School of Physical & Mathematical Sciences, Nanyang Technological University, Singapore 637371

† Present address: Division of Chemistry and Biological Chemistry, Nanyang Technological University, Singapore 637616. Email: LaiYoongGoh@ntu.edu.sg . Fax: +65 6316 6984

‡ Email: boere@uleth.ca. Fax: +1-403-329-2057

Electronic Supplementary Materials

Figure S1	Temperature dependence of the ¹ H NMR spectra of 3d between 200 and 300 K with details of assignment of signals to isomers	p: 2
Figure S2	Diagram showing for 3d all the AA'BB' DNMR line-fits (left) with experimental spectra (center) and the superposition of the fits on the data (right)	p: 3
Figure S3	Diagram showing for 3d all the Cp region DNMR linefits (left) with experimental spectra (center) and the superposition of the fits on the data (right)	p: 4
Figure S4	Plots of <i>lnK</i> vs. 1/T from the Cp signals of 4d	p: 5
Figure S5	Eyring plots for the exchange rate study of 3d from the Cp spectral region	p: 5
Figure S6	Atom-labels and full geometric details for the optimized (a) <i>exo</i> isomer (-2409.1423602 Hartree) and (b) <i>endo</i> isomer (-2409.143318 Hartree) from B3PW91/6-311+G(2d,2p)// B3PW91/6-31G(d) calculations	p: 6
Figure S7	Enlarged rendering of the CV scans from Figure 5	p: 7
Figure S8	Diagrams showing the four dimers of 2d and the unit cell packing	p: 8
Table S1	Equilibrium Constants from the DNMR Study of 3d , Eyring Analysis	p: 9
Table S2	Rate data from the DNMR study on 3d , Eyring Analysis	p: 10
Table S3	Summary of Dynamic NMR Results	p: 11

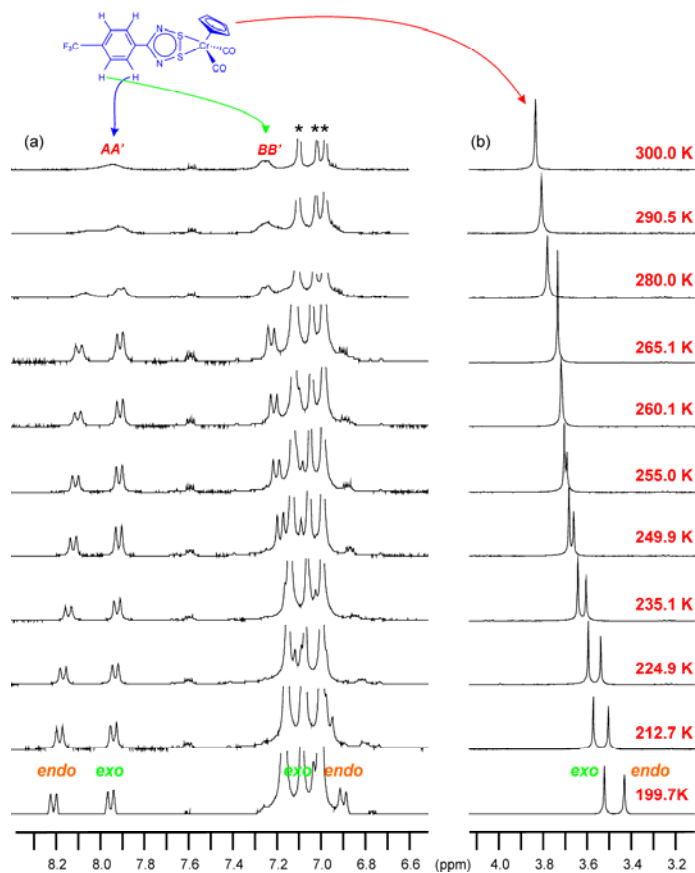


Figure S1. Stacked plots of ^1H NMR traces in the (a) AA' BB' aromatic H and (b) Cp regions of **3d** over the range 200 – 300 K. The aromatic region has been scaled up in the vertical sense by a considerable amount, and the residual d_8 -toluene signals, marked by $*$, have been cut short. The AA' and BB' signals of the aromatic ring are indicated, and the assignment of the signals to the different isomers is also indicated. Note the large temperature dependence of the signals from both ligands w.r.t. the residual solvent signals from toluene- d_8 , with the result that the low-field BB' signals move through the solvent lines over the 100 K temperature range.

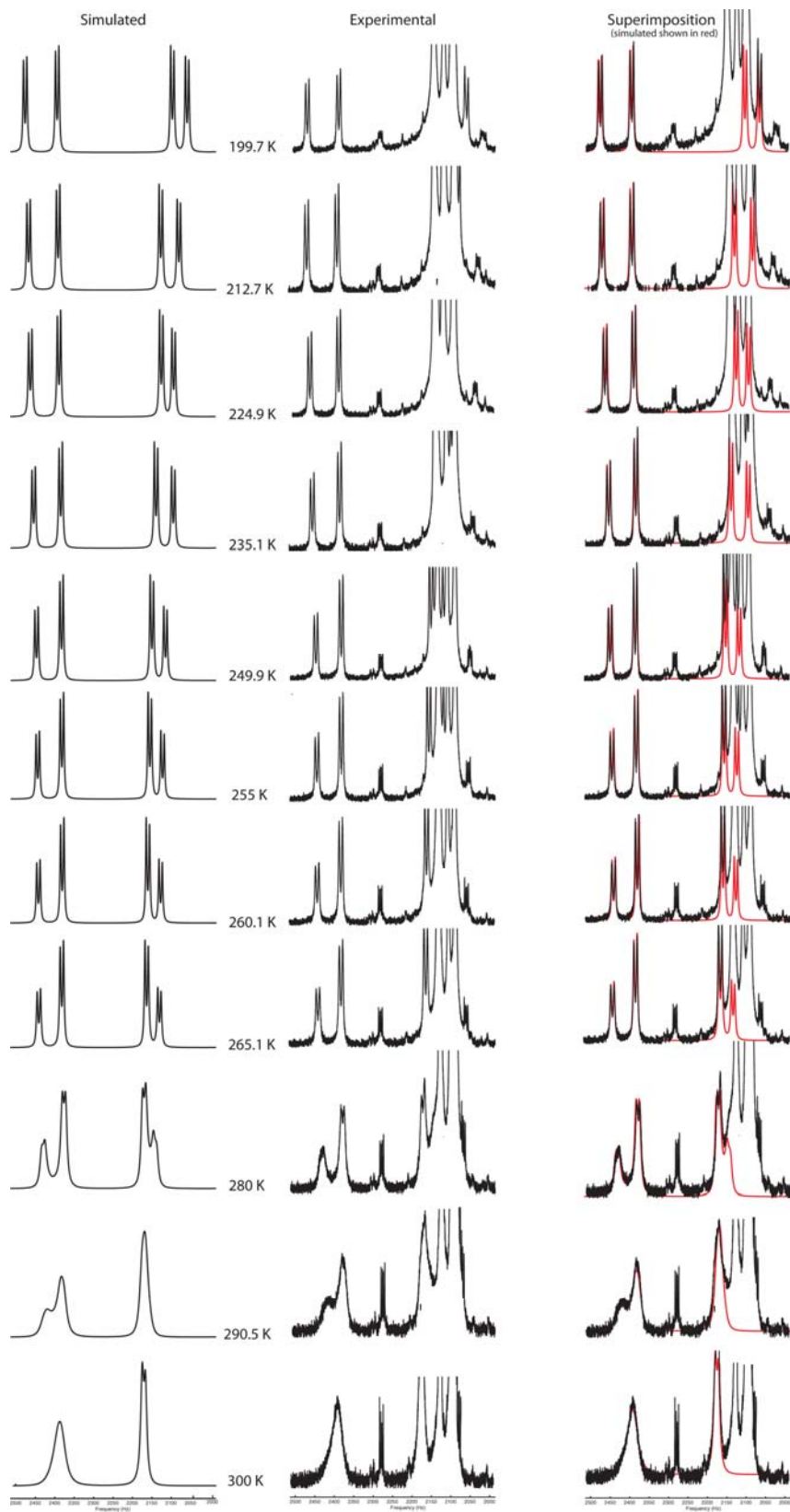


Figure S2. Diagram showing for **3d** all the AA'BB' DNMR linefits (left) with experimental spectra (center) and the superposition of the fits on the data (right).

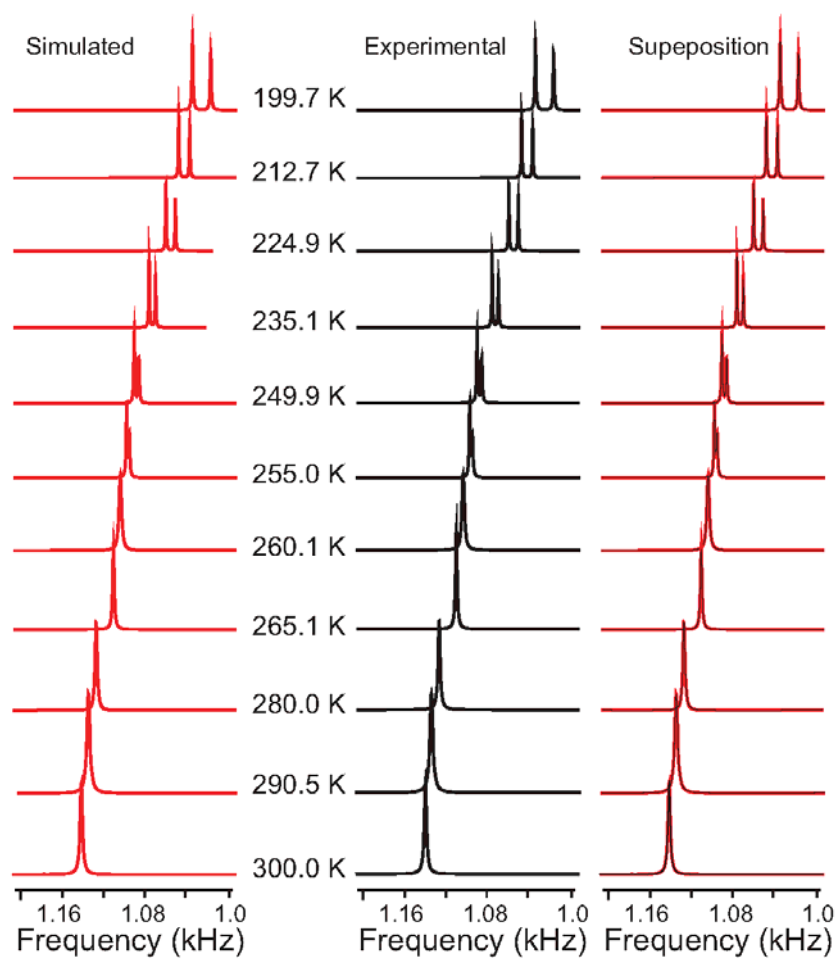


Figure S3. Diagram showing for **3d** all the Cp region DNMR linefits (left) with experimental spectra (center) and the superposition of the fits on the data (right).

(a)

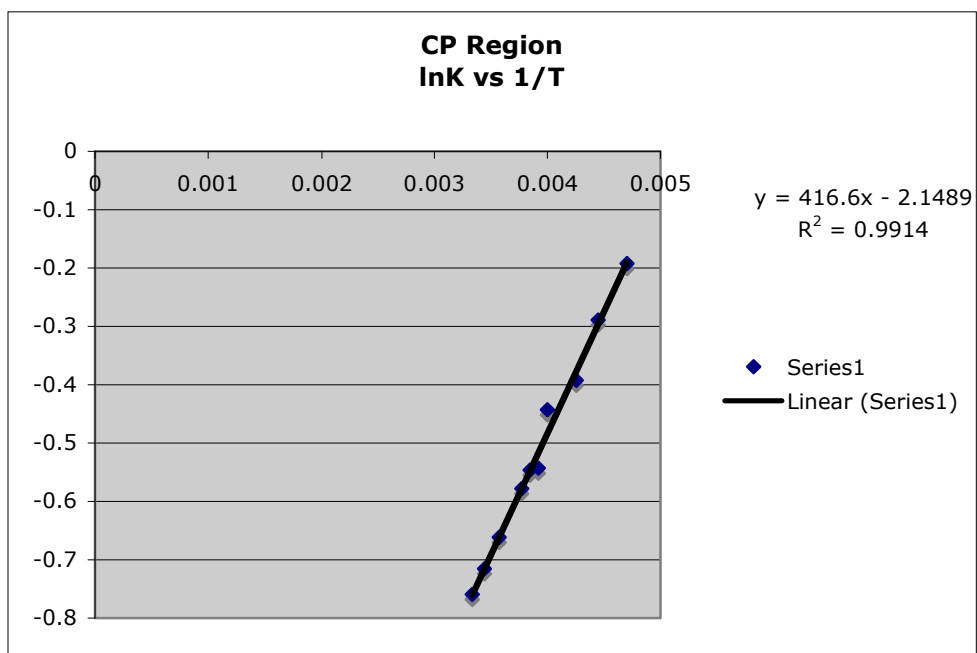


Figure S4 – Plots of $\ln K$ vs. $1/T$ from the Cp signals of **4d**

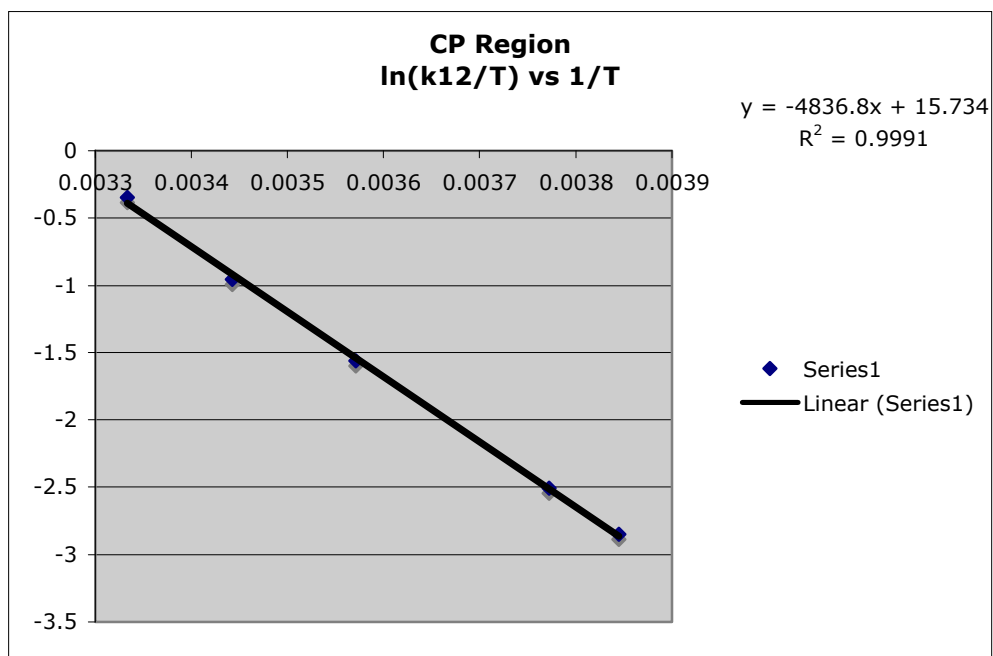
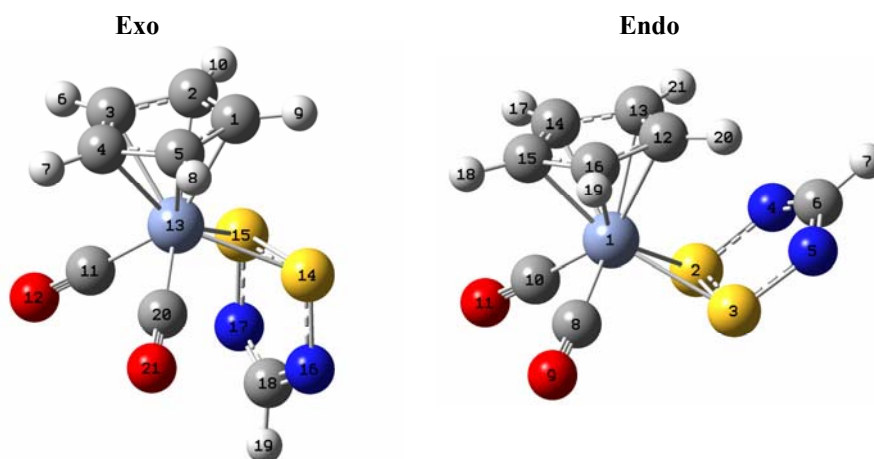


Figure S5 Eyring plots for the exchange rate study of **3d** from the Cp spectral region.



Exo isomer (-2409.1423602 Hartree):

Distances, Å		Angles, °	
Cr—S14	2.37207	Cr—S14—N16	112.99488
Cr—C11	1.84126	Cr—S14—S16	62.2244
Cr—C1	2.22851	S15—S14—N16	92.63249
Cr—C4	2.14886	S14—N16—C18	114.23057
Cr—C5	2.17596	N16—C18—N17	125.23303
S14—S15	2.21081	S15—Cr—C11	84.56538
S14—N16	1.64776	C11—Cr—C20	81.87248
N16—C18	1.33013	S14—Cr—C1	85.02349
C11—O12	1.15827	S14—Cr—C5	105.5517
C1—C2	1.41912	S14—Cr—C4	143.97551
C1—C5	1.42011	C2—C1—C5	108.19446
C5—C4	1.42742	C1—C5—C4	107.92887
		C5—C4—C3	107.75051

Endo isomer (-2409.143318 Hartree):

Distances, Å		Angles, °	
Cr—S2	2.3878	Cr—S2—N4	112.80999
Cr—C8	1.83815	Cr—S2—S3	62.47819
Cr—C12	2.22066	S3—S2—N4	92.76847
Cr—C15	2.15279	S2—N4—C6	114.22321
Cr—C16	2.17846	N4—C6—N5	125.38998
S2—S3	2.20210	S2—Cr—C10	81.37219
S2—N4	1.65417	C8—Cr—C10	81.66016
N4—C6	1.32903	S2—Cr—C13	90.70312
C8—O9	1.15954	S2—Cr—C14	109.48207
C12—C13	1.41806	S2—Cr—C15	147.94706
C12—C16	1.41959	C12—C13—C14	108.21153
C15—C16	1.42750	C13—C14—C15	107.93714
		C14—C15—C16	107.70257

Figure S6. Atom-labels and full geometric details for the optimized (a) *exo* isomer (-2409.1423602 Hartree) and (b) *endo* isomer (-2409.143318 Hartree) from B3PW91/6-311+G(2d,2p)//B3PW91/6-31G(d) calculations. The **endo** isomer is more stable by 2.51 kJ/mol

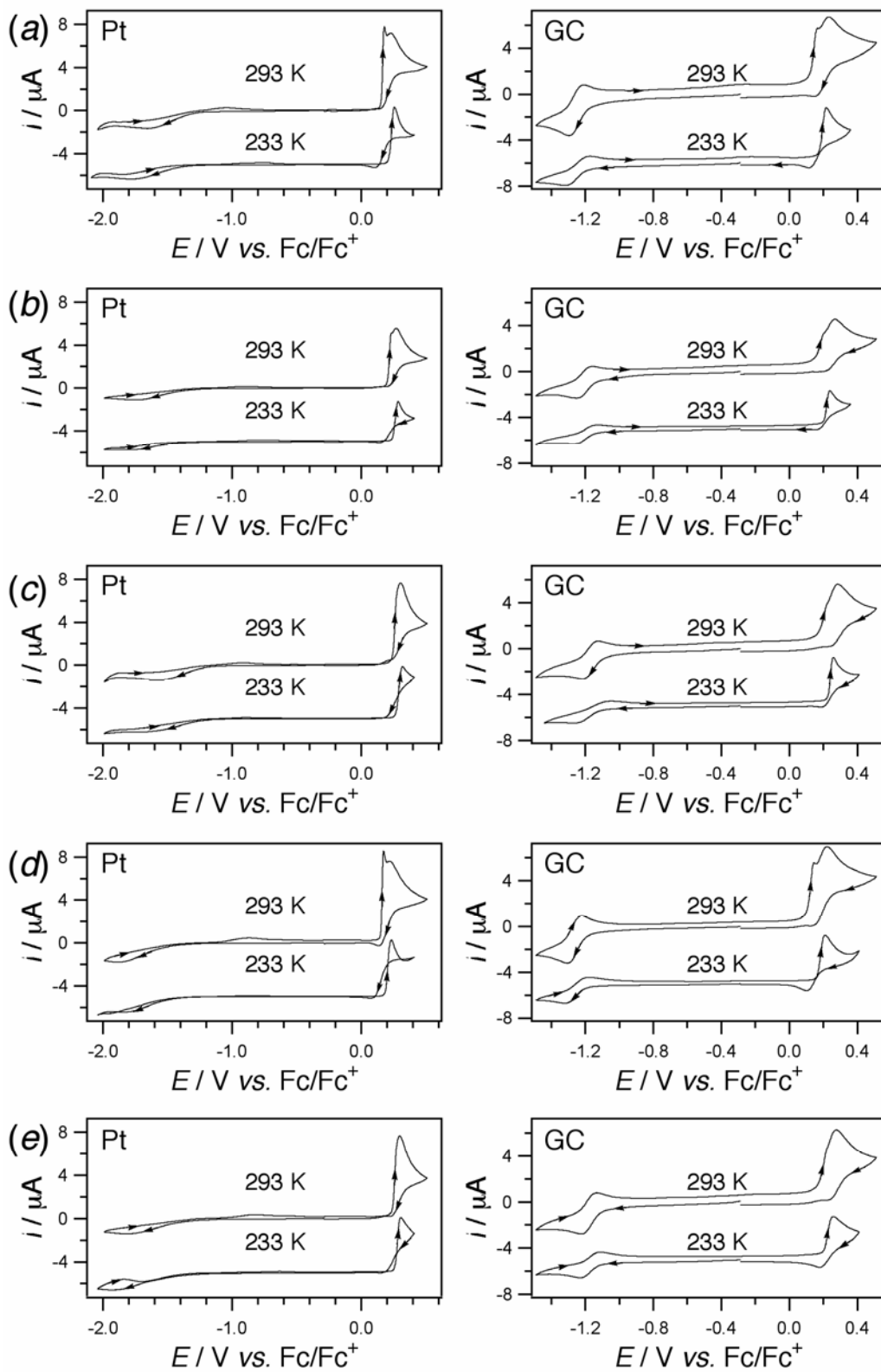
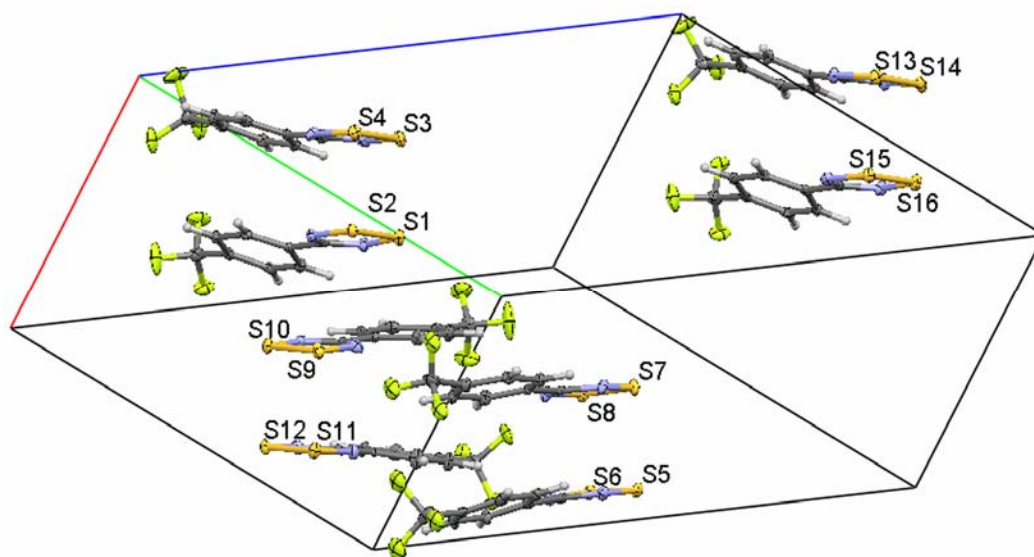
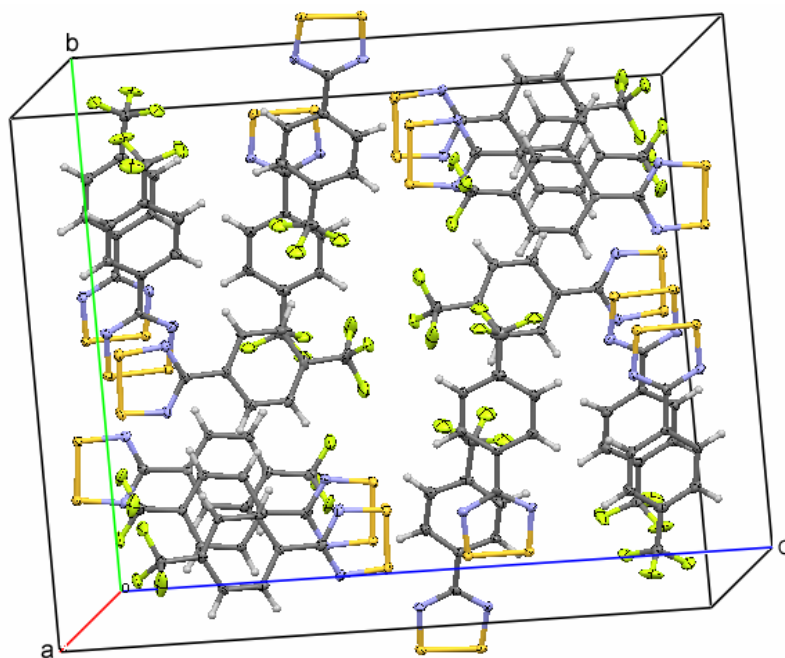


Figure S7. Enlarged rendering of the CV scans from Figure 5



(a)



(b)

Figure S8. (a) View of the unit cell of the reported crystal structure of **2d** approximately in the $[1 -1 1]$ direction showing the four unique dimers in the asymmetric unit. (b) Full unit cell packing diagram for the crystal structure of **2d** viewed approximately in the $[-1 0 0]$ direction.

Table S1

Equilibrium Constants from the DNMR Study of 3d

T, K	K (CP)
199.7	0.83
212.7	0.825
224.9	0.749
235.1	0.675
249.9	0.642
255	0.581
260.1	0.579
265.1	0.561
280	0.516
290.5	0.489
300	0.468

Eyring Analysis

S.E.	0.035275709
R ²	0.971910168
ΔH , kJ/mol	-3.1 _(0.2)
ΔS^* , kJ/molK	-0.017 _(0.0014)
ΔG^{**} (298), kJ/mol	1.82 _(0.2)
ΔG^{**} (300), kJ/mol	2 _(0.2)

* Error in ΔS extrapolated to origin

** Error in ΔG include that of $\Delta H + \Delta S$ as $\sigma_{\Delta G} = \sqrt{\sigma_{\Delta H}^2 + T^2 \cdot \sigma_{\Delta S}^2}$

Table S2

Rate data from the DNMR study on 3d

T, K	k12 (CP)
199.7	0.001
212.7	0.01
224.9	0.01
235.1	0.2
249.9	0.28
255	1
260.1	15.08
265.1	21.62
280	58.7
290.5	111.8
300	212

Eyring analysis

S.E.	0.035275709
R ²	0.971910168
ΔH , kJ/mol	39.06 _(0.031)
ΔS^* , kJ/molK	-0.071 _(2.2*10⁻⁴)
ΔG^{**} (300), kJ/mol	60.23 _(0.03)
Ea, kJ/mol	42.5 _(0.1)
ΔG^{\ddagger} (300), kJ/mol	60.13 _(0.24)

[‡] Calculated directly from exchange rates at 300⁰C

* Error in ΔS extrapolated to origin

** Error in ΔG include that of $\Delta H + \Delta S$ as $\sigma_{\Delta G} = \sqrt{\sigma_{\Delta H}^2 + T^2 \cdot \sigma_{\Delta S}^2}$

Table S3 Summary of Dynamic NMR Results ^a

Aromatic signals				Cp signals			
ΔH°	-1.39	n ^b	11	ΔH°	-3.1	n ^b	11
$\sigma\Delta H^\circ$	0.003	R ^c	0.99998	$\sigma\Delta H^\circ$	-0.2	R ^c	0.98586
ΔS°	-7.2	R ² ^d	0.99996	ΔS°	-17	R ² ^d	0.97191
$\sigma\Delta S^\circ$	0.02	St. Error ^e	0.57	$\sigma\Delta S^\circ$	1.4	St. Error ^e	35
ΔG°_{298}	0.76	—	—	ΔG°_{298}	1.82	—	—
$\sigma\Delta G^\circ_{298}$	-0.004	—	—	$\sigma\Delta G^\circ_{298}$	-0.62	—	—
ΔH^\ddagger	76.89	n ^b	4	ΔH^\ddagger	40.21	n ^b	5
$\sigma\Delta H^\ddagger$	4.37	R ^c	0.99679	$\sigma\Delta H^\ddagger$	0.70	R ^c	0.99999
ΔS^\ddagger	60.4	R ² ^d	0.99359	ΔS^\ddagger	-66.8	R ² ^d	0.99999
$\sigma\Delta S^\ddagger$	21.8	St. Error ^e	172	$\sigma\Delta S^\ddagger$	3.6	St. Error ^e	1.58
ΔG^\ddagger_{298}	58.89	—	—	ΔG^\ddagger_{298}	60.1	—	—
$\sigma\Delta G^\ddagger_{298}$	6.3	—	—	$\sigma\Delta G^\ddagger_{298}$	0.1	—	—

^a All ΔH and ΔG values in kJ mol⁻¹; ΔS values are J K⁻¹ mol⁻¹.

^b Number of traces used in the analysis. Note that all traces could be used to establish the equilibrium constant, but only those showing effects of exchange were suitable for establishing the activation parameters.

^c Residual in the linear regression analysis (slope).

^d Residual in the linear regression analysis (intercept).

^e Statistical error, see Experimental section.

Coupling of CpCr(CO)₃ and Heterocyclic Dithiadiazolyl Radicals. Synthetic, X-ray diffraction, dynamic NMR, EPR, CV and DFT studies.

Hiu Fung Lau,^(a) Pearly Chwee Ying Ang,^(a) Victor Wee Lin Ng,^(a) Seah Ling Kuan,^(a) Lai Yoong Goh,^{(a)*†} Alexey S. Borisov,^(b) Paul Hazendonk,^(b) Tracey L. Roemmele,^(b) René T. Boéré,^{(b)*‡} and Richard D. Webster^(c)

^(a) Department of Chemistry, National University of Singapore, Kent Ridge, Singapore 119260

^(b) Department of Chemistry and Biochemistry, University of Lethbridge, Lethbridge, Alberta, Canada T1K 3M4

^(c) Division of Chemistry and Biological Chemistry, School of Physical & Mathematical Sciences, Nanyang Technological University, Singapore 637371

† Present address: Division of Chemistry and Biological Chemistry, Nanyang Technological University, Singapore 637616. Email: LaiYoongGoh@ntu.edu.sg . Fax: +65 6316 6984

‡ Email: boere@uleth.ca. Fax: +1-403-329-2057

Electronic Supplementary Materials

Figure S1	Temperature dependence of the ¹ H NMR spectra of 3d between 200 and 300 K with details of assignment of signals to isomers	p: 2
Figure S2	Diagram showing for 3d all the AA'BB' DNMR line-fits (left) with experimental spectra (center) and the superposition of the fits on the data (right)	p: 3
Figure S3	Diagram showing for 3d all the Cp region DNMR linefits (left) with experimental spectra (center) and the superposition of the fits on the data (right)	p: 4
Figure S4	Plots of <i>lnK</i> vs. 1/T from the Cp signals of 4d	p: 5
Figure S5	Eyring plots for the exchange rate study of 3d from the Cp spectral region	p: 5
Figure S6	Atom-labels and full geometric details for the optimized (a) <i>exo</i> isomer (-2409.1423602 Hartree) and (b) <i>endo</i> isomer (-2409.143318 Hartree) from B3PW91/6-311+G(2d,2p)// B3PW91/6-31G(d) calculations	p: 6
Figure S7	Enlarged rendering of the CV scans from Figure 5	p: 7
Figure S8	Diagrams showing the four dimers of 2d and the unit cell packing	p: 8
Table S1	Equilibrium Constants from the DNMR Study of 3d , Eyring Analysis	p: 9
Table S2	Rate data from the DNMR study on 3d , Eyring Analysis	p: 10
Table S3	Summary of Dynamic NMR Results	p: 11

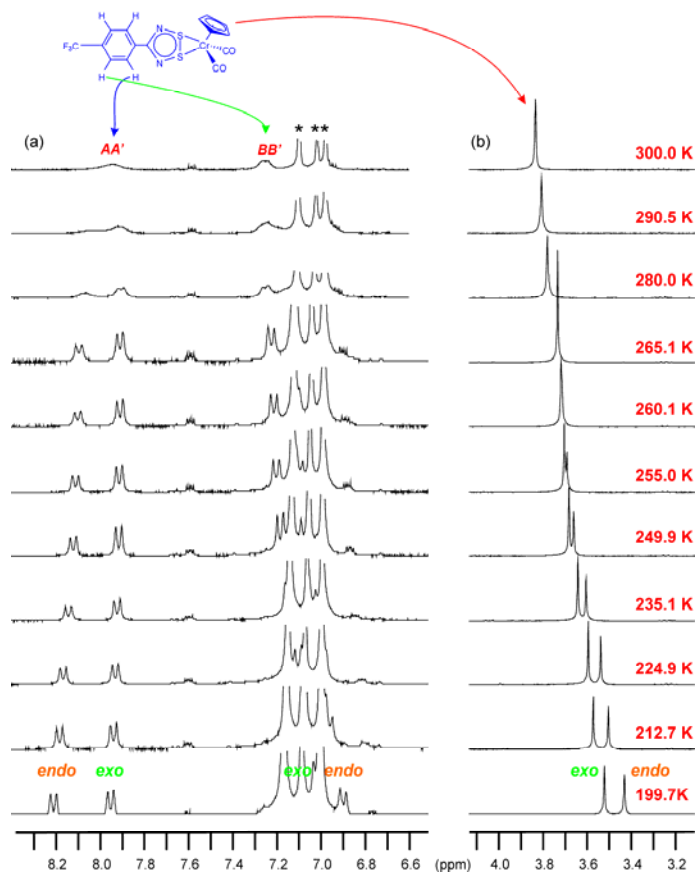


Figure S1. Stacked plots of ^1H NMR traces in the (a) AA' BB' aromatic H and (b) Cp regions of **3d** over the range 200 – 300 K. The aromatic region has been scaled up in the vertical sense by a considerable amount, and the residual d_8 -toluene signals, marked by *, have been cut short. The AA' and BB' signals of the aromatic ring are indicated, and the assignment of the signals to the different isomers is also indicated. Note the large temperature dependence of the signals from both ligands w.r.t. the residual solvent signals from toluene- d_8 , with the result that the low-field BB' signals move through the solvent lines over the 100 K temperature range.

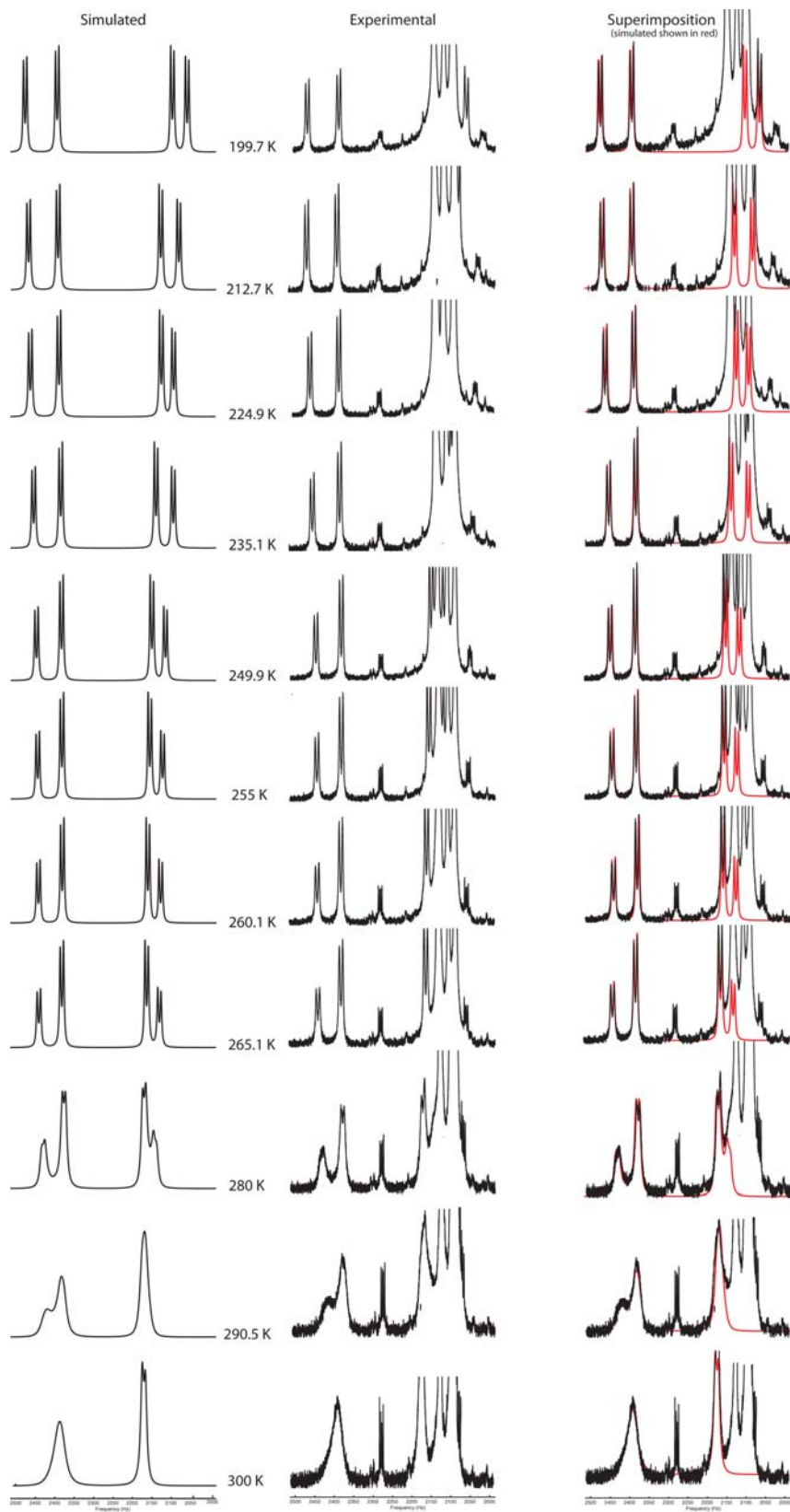


Figure S2. Diagram showing for **3d** all the AA'BB' DNMR linefits (left) with experimental spectra (center) and the superposition of the fits on the data (right).

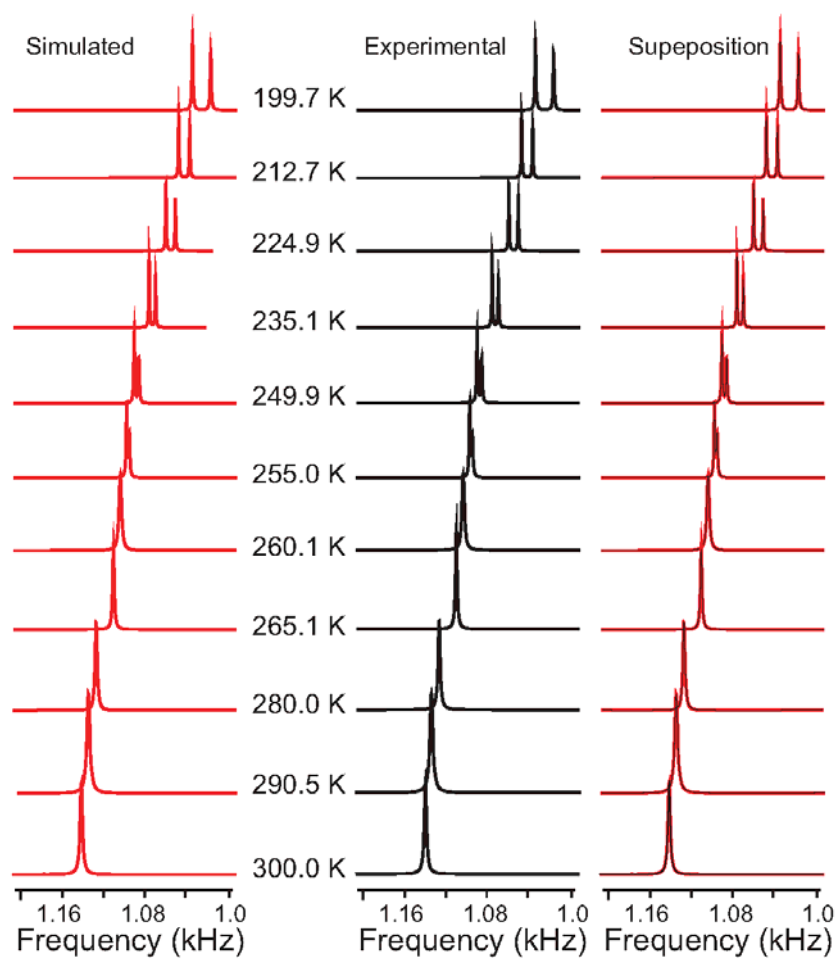


Figure S3. Diagram showing for **3d** all the Cp region DNMR linefits (left) with experimental spectra (center) and the superposition of the fits on the data (right).

(a)

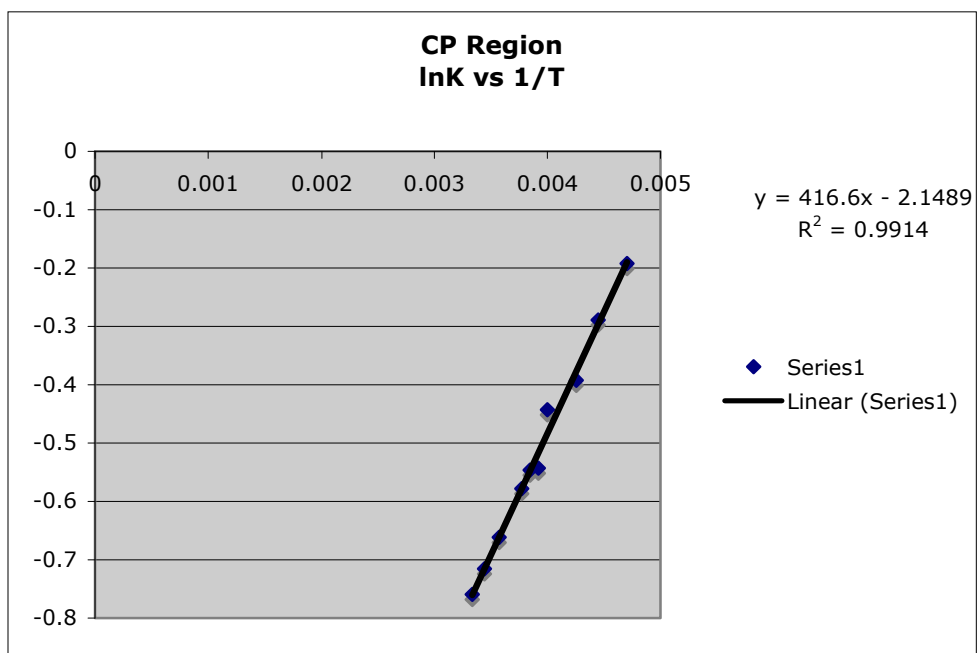


Figure S4 – Plots of $\ln K$ vs. $1/T$ from the Cp signals of **4d**

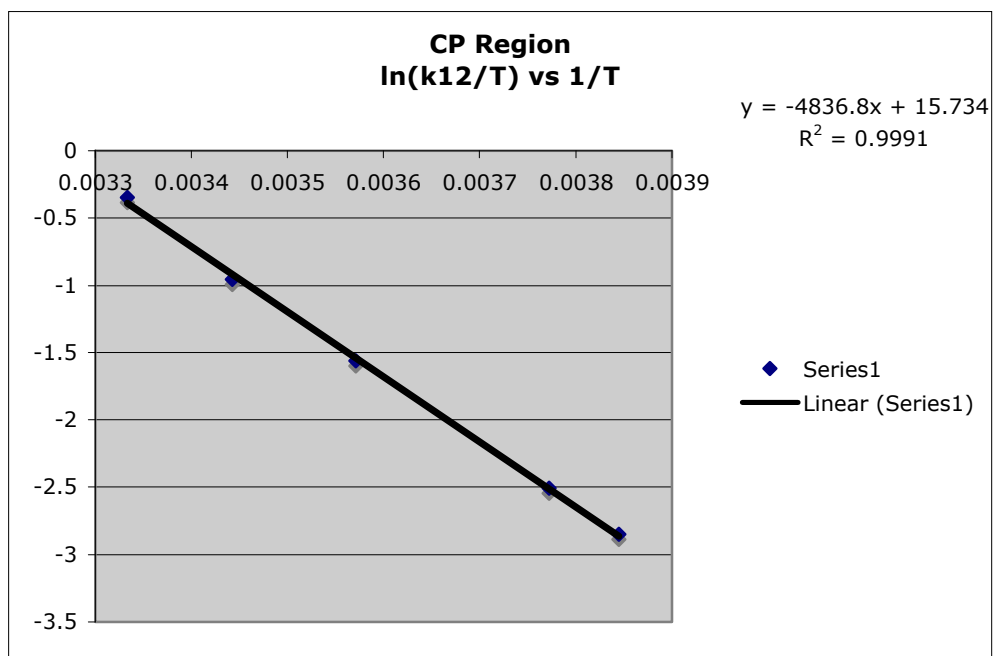
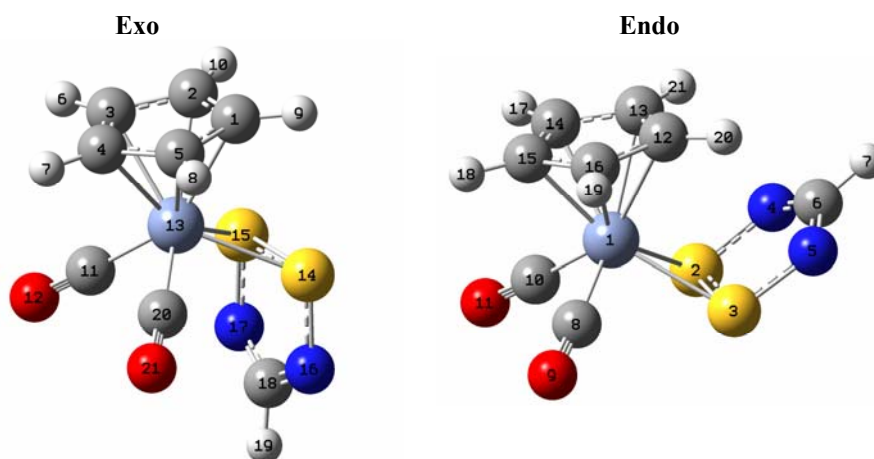


Figure S5 Eyring plots for the exchange rate study of **3d** from the Cp spectral region.



Exo isomer (-2409.1423602 Hartree):

Distances, Å		Angles, °	
Cr—S14	2.37207	Cr—S14—N16	112.99488
Cr—C11	1.84126	Cr—S14—S16	62.2244
Cr—C1	2.22851	S15—S14—N16	92.63249
Cr—C4	2.14886	S14—N16—C18	114.23057
Cr—C5	2.17596	N16—C18—N17	125.23303
S14—S15	2.21081	S15—Cr—C11	84.56538
S14—N16	1.64776	C11—Cr—C20	81.87248
N16—C18	1.33013	S14—Cr—C1	85.02349
C11—O12	1.15827	S14—Cr—C5	105.5517
C1—C2	1.41912	S14—Cr—C4	143.97551
C1—C5	1.42011	C2—C1—C5	108.19446
C5—C4	1.42742	C1—C5—C4	107.92887
		C5—C4—C3	107.75051

Endo isomer (-2409.143318 Hartree):

Distances, Å		Angles, °	
Cr—S2	2.3878	Cr—S2—N4	112.80999
Cr—C8	1.83815	Cr—S2—S3	62.47819
Cr—C12	2.22066	S3—S2—N4	92.76847
Cr—C15	2.15279	S2—N4—C6	114.22321
Cr—C16	2.17846	N4—C6—N5	125.38998
S2—S3	2.20210	S2—Cr—C10	81.37219
S2—N4	1.65417	C8—Cr—C10	81.66016
N4—C6	1.32903	S2—Cr—C13	90.70312
C8—O9	1.15954	S2—Cr—C14	109.48207
C12—C13	1.41806	S2—Cr—C15	147.94706
C12—C16	1.41959	C12—C13—C14	108.21153
C15—C16	1.42750	C13—C14—C15	107.93714
		C14—C15—C16	107.70257

Figure S6. Atom-labels and full geometric details for the optimized (a) *exo* isomer (-2409.1423602 Hartree) and (b) *endo* isomer (-2409.143318 Hartree) from B3PW91/6-311+G(2d,2p)//B3PW91/6-31G(d) calculations. The **endo** isomer is more stable by 2.51 kJ/mol

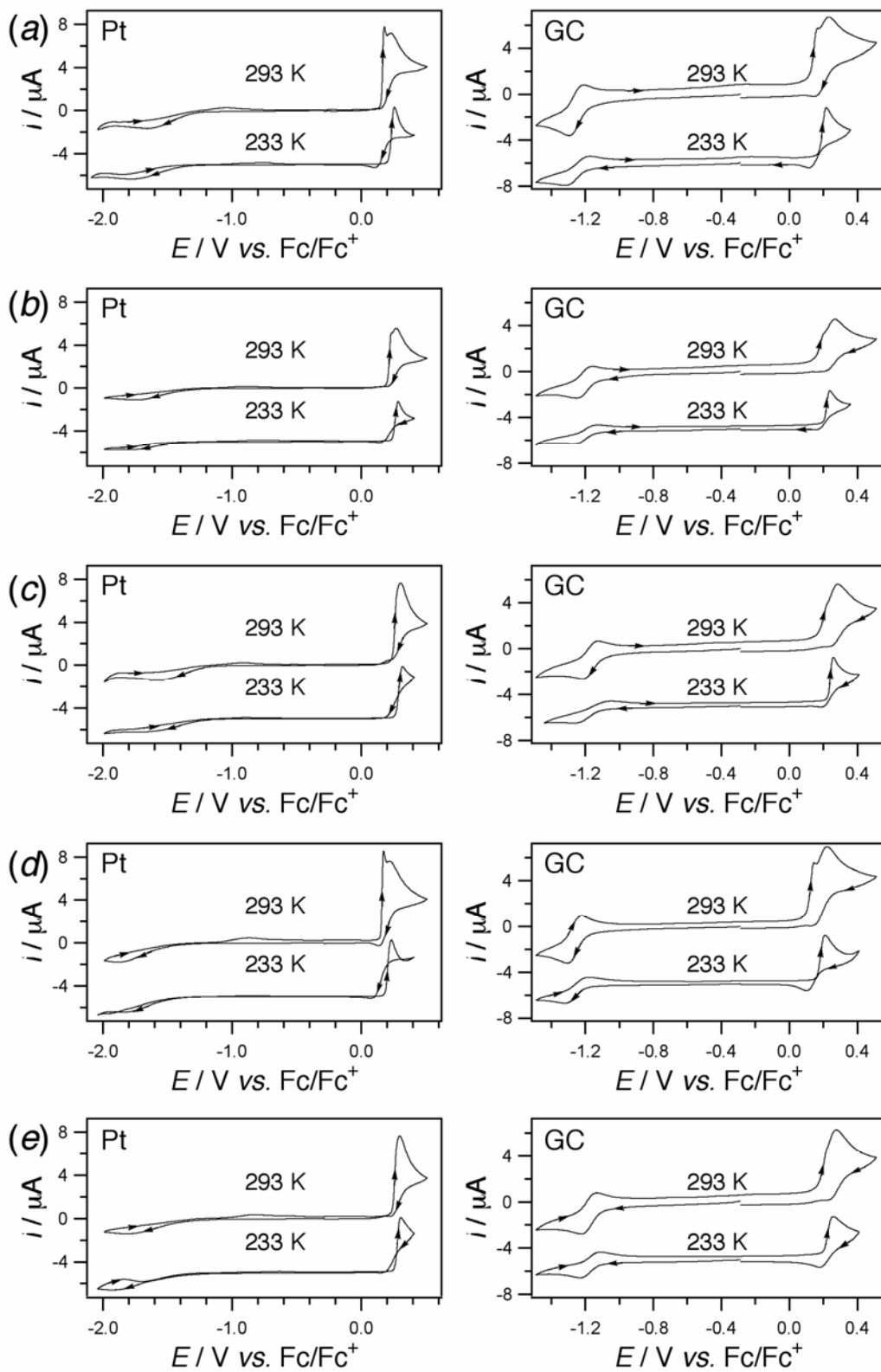
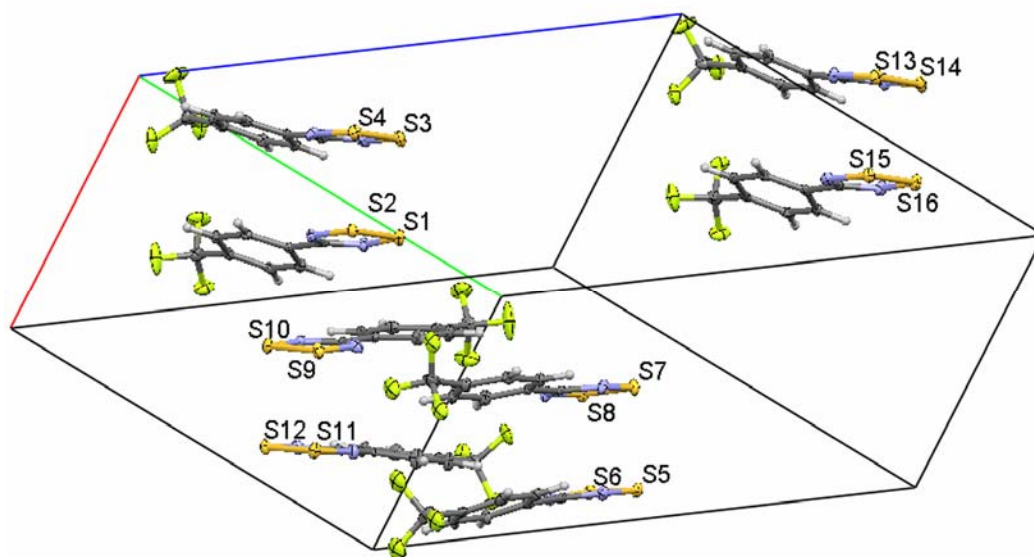
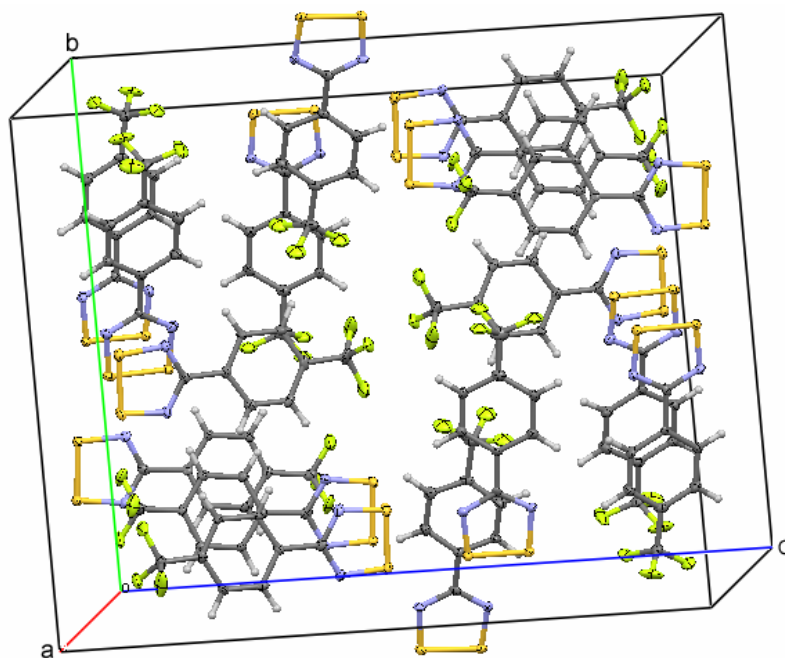


Figure S7. Enlarged rendering of the CV scans from Figure 5



(a)



(b)

Figure S8. (a) View of the unit cell of the reported crystal structure of **2d** approximately in the $[1 -1 1]$ direction showing the four unique dimers in the asymmetric unit. (b) Full unit cell packing diagram for the crystal structure of **2d** viewed approximately in the $[-1 0 0]$ direction.

Table S1

Equilibrium Constants from the DNMR Study of 3d

T, K	K (CP)
199.7	0.83
212.7	0.825
224.9	0.749
235.1	0.675
249.9	0.642
255	0.581
260.1	0.579
265.1	0.561
280	0.516
290.5	0.489
300	0.468

Eyring Analysis

S.E.	0.035275709
R ²	0.971910168
ΔH , kJ/mol	-3.1 _(0.2)
ΔS^* , kJ/molK	-0.017 _(0.0014)
ΔG^{**} (298), kJ/mol	1.82 _(0.2)
ΔG^{**} (300), kJ/mol	2 _(0.2)

* Error in ΔS extrapolated to origin

** Error in ΔG include that of $\Delta H + \Delta S$ as $\sigma_{\Delta G} = \sqrt{\sigma_{\Delta H}^2 + T^2 \cdot \sigma_{\Delta S}^2}$

Table S2

Rate data from the DNMR study on 3d

T, K	k12 (CP)
199.7	0.001
212.7	0.01
224.9	0.01
235.1	0.2
249.9	0.28
255	1
260.1	15.08
265.1	21.62
280	58.7
290.5	111.8
300	212

Eyring analysis

S.E.	0.035275709
R ²	0.971910168
Δ H, kJ/mol	39.06 _(0.031)
Δ S*, kJ/molK	-0.071 _(2.2*10⁻⁴)
Δ G** (300), kJ/mol	60.23 _(0.03)
Ea, kJ/mol	42.5 _(0.1)
Δ G [‡] (300), kJ/mol	60.13 _(0.24)

[‡] Calculated directly from exchange rates at 300⁰C

* Error in Δ S extrapolated to origin

** Error in Δ G include that of Δ H + Δ S as $\sigma_{\Delta G} = \sqrt{\sigma_{\Delta H}^2 + T^2 \cdot \sigma_{\Delta S}^2}$

Table S3 Summary of Dynamic NMR Results ^a

Aromatic signals				Cp signals			
ΔH°	-1.39	n ^b	11	ΔH°	-3.1	n ^b	11
$\sigma\Delta H^\circ$	0.003	R ^c	0.99998	$\sigma\Delta H^\circ$	-0.2	R ^c	0.98586
ΔS°	-7.2	R ² ^d	0.99996	ΔS°	-17	R ² ^d	0.97191
$\sigma\Delta S^\circ$	0.02	St. Error ^e	0.57	$\sigma\Delta S^\circ$	1.4	St. Error ^e	35
ΔG°_{298}	0.76	—	—	ΔG°_{298}	1.82	—	—
$\sigma\Delta G^\circ_{298}$	-0.004	—	—	$\sigma\Delta G^\circ_{298}$	-0.62	—	—
ΔH^\ddagger	76.89	n ^b	4	ΔH^\ddagger	40.21	n ^b	5
$\sigma\Delta H^\ddagger$	4.37	R ^c	0.99679	$\sigma\Delta H^\ddagger$	0.70	R ^c	0.99999
ΔS^\ddagger	60.4	R ² ^d	0.99359	ΔS^\ddagger	-66.8	R ² ^d	0.99999
$\sigma\Delta S^\ddagger$	21.8	St. Error ^e	172	$\sigma\Delta S^\ddagger$	3.6	St. Error ^e	1.58
ΔG^\ddagger_{298}	58.89	—	—	ΔG^\ddagger_{298}	60.1	—	—
$\sigma\Delta G^\ddagger_{298}$	6.3	—	—	$\sigma\Delta G^\ddagger_{298}$	0.1	—	—

^a All ΔH and ΔG values in kJ mol^{-1} ; ΔS values are $\text{J K}^{-1} \text{mol}^{-1}$.

^b Number of traces used in the analysis. Note that all traces could be used to establish the equilibrium constant, but only those showing effects of exchange were suitable for establishing the activation parameters.

^c Residual in the linear regression analysis (slope).

^d Residual in the linear regression analysis (intercept).

^e Statistical error, see Experimental section.